Downloaded from jgp.rupress.org on April 1, 2016

Reverberation of excitation in neuronal networks interconnected through voltage-gated gap junction channels

Kestutis Maciunas,¹ Mindaugas Snipas,^{1,2} Nerijus Paulauskas,¹ and Feliksas F. Bukauskas^{1,3}

We combined Hodgkin–Huxley equations and gating models of gap junction (GJ) channels to simulate the spread of excitation in two-dimensional networks composed of neurons interconnected by voltage-gated GJs. Each GJ channel contains two fast and slow gates, each exhibiting current–voltage (I-V) rectification and gating properties that depend on transjunctional voltage (V_j). The data obtained show how junctional conductance (g_j), which is necessary for synchronization of the neuronal network, depends on its size and the intrinsic firing rate of neurons. A phase shift between action potentials (APs) of neighboring neurons creates bipolar, short-lasting V_j spikes of approximately ± 100 mV that induce V_j gating, leading to a small decay of g_j , which can accumulate into larger decays during bursting activity of neurons. We show that I-V rectification of GJs in local regions of the two-dimensional network of neurons can lead to unidirectional AP transfer and consequently to reverberation of excitation. This reverberation can be initiated by a single electrical pulse and terminated by a low-amplitude pulse applied in a specific window of reverberation cycle. Thus, the model accounts for the influence of dynamically modulatable electrical synapses in shaping the function of a neuronal network and the formation of reverberation, which, as proposed earlier, may be important for the development of short-term memory and its consolidation into long-term memory.

INTRODUCTION

The Journal of General Physiology

In models describing synchronization of neuronal networks or the spread of excitation in excitable structures, cell-to-cell communication through gap junction (GJ) channels composed of the connexin (Cx) protein was typically defined as having constant conductance (see online database of models that contain GJs at https://senselab .med.yale.edu/ModelDB/ModelList.cshtml?id=114107 &describe=yes&celldescr=&). It is well established that GJ communication (GJC) exhibits changes caused by gating by voltage and chemical reagents as well as current-voltage (I-V) rectification; however, neither of these properties were accounted for during simulations of networks formed of neurons, cardiomyocytes, or other types of excitable cells. GJC plays an important role in the propagation of excitation in the heart, communication between neurons, metabolic exchange between cells in most organs and tissues, including the lens (which lacks blood circulation), and organ formation during development or regulation of cell proliferation (Bukauskas and Verselis, 2004; González et al., 2007).

Electrical synapses between mammalian neurons are preferentially composed of Cx36, which is commonly expressed by neurons throughout the central nervous system (Connors and Long, 2004; Söhl et al., 2005).

Correspondence to Feliksas F. Bukauskas: feliksas.bukauskas@einstein.yu.edu Abbreviations used in this paper: 16SM, 16-state model of GJ channel gating; aHC, apposed hemichannel; AP, action potential; GJ, gap junction; GJC, GJ communication; H-H, Hodgkin–Huxley; MC16SM, Markov chain 16SM; S16SM, stochastic 16SM.

Many roles for electrical synapses have been documented, such as metabolic communication, synchronization of neuronal networks, and memory formation (Bennett and Zukin, 2004; Bissiere et al., 2011). Also, electrical synapses rectify and cause asymmetry of signal transfer (Furshpan and Potter, 1959; Auerbach and Bennett, 1969; Phelan et al., 2008; Rash et al., 2013). Modulation of electrical synapses can occur by different factors, including phosphorylation (Ouyang et al., 2005; Cachope et al., 2007; Alev et al., 2008), changes in pH (González-Nieto et al., 2008), intracellular concentration of divalent cations (Palacios-Prado et al., 2013, 2014), and activity-dependent long-term depression (Haas et al., 2011).

A property that appears to be common to all 21 members of the Cx family is the sensitivity of junctional conductance (g_j) to transjunctional voltage (V_j) . Single-channel studies have shown that V_j causes channels to close to a subconductance (residual) state with fast gating transitions (<1 ms; Bukauskas and Weingart, 1994; Moreno et al., 1994). It was shown that V_j as well as chemical uncouplers can also induce gating transitions to the fully closed state and that these transitions are slow, >10 ms (Bukauskas and Weingart, 1994; Bukauskas and Peracchia, 1997). Gating to different levels via distinct fast and slow gating transitions led to the

© 2016 Maciunas et al. This article is distributed under the terms of an Attribution–Non-commercial–Share Alike–No Mirror Sites license for the first six months after the publication date (see http://www.rupress.org/terms). After six months it is available under a Creative Commons License (Attribution–Noncommercial–Share Alike 3.0 Unported license, as described at http://creativecommons.org/licenses/by-nc-sa/3.0/).

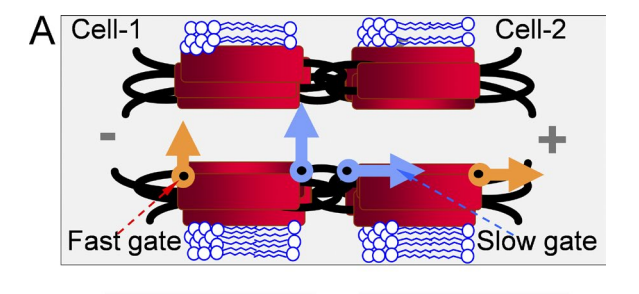
¹Institute of Cardiology, Lithuanian University of Health Sciences, 50009 Kaunas, Lithuania

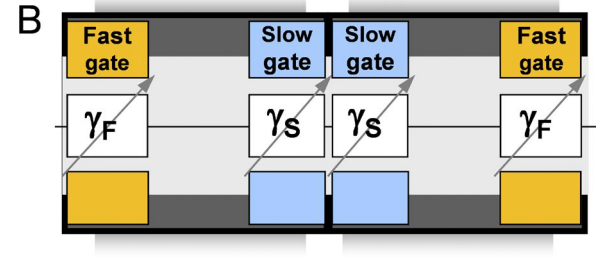
²Department of Mathematical Modelling, Kaunas University of Technology, 51368 Kaunas, Lithuania

³Dominick P. Purpura Department of Neuroscience, Albert Einstein College of Medicine, New York, NY 10461

suggestion that there are two distinct $V_{\bar{l}}$ sensitive gates, termed fast and slow (or loop gating) mechanisms (Bukauskas and Verselis, 2004). Earlier, gating properties of GI channels were described by using the Boltzmann function (Harris et al., 1981), which assumes that GJ channels have two states: open and fully closed. It was presumed that each hemichannel of the GJ channel gates only when the apposed (or docked) hemichannel (aHC) is open and that all V_i falls on the gated hemichannel, whereas in fact V_i falls on both hemichannels and they can gate at the same time. Furthermore, there were several attempts to describe V_i gating of GJs with a multistate approach, which provided more detailed descriptions of gating processes (Vogel and Weingart, 1998; Ramanan et al., 1999; Chen-Izu et al., 2001). The discovery of fast and slow gates (Fig. 1, A and B) motivated us to develop stochastic 4- and 16-state models of GI channel gating (Paulauskas et al., 2009, 2012).

However, all previous models were adopted to study GJC between two individual cells. Here, we present a model describing a 2-D network of neurons, each exhibiting excitability according to Hodgkin–Huxley (H-H)





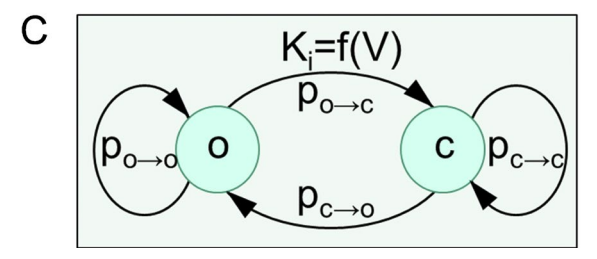


Figure 1. GJ channels contain fast and slow gating mechanisms. (A) Schematic of the GJ channel illustrating fast gates (orange) that close the channel partially to the so-called residual state and the slow gates (blue) that close the channel fully. (B) Schematic of the GJ channel is combined with the principal electrical scheme composed of four variable resistances in series attributed to the fast (γ_F) and slow (γ_S) gates. (C) A schematic of possible transitions of the gate, which has open (o) and closed (c) states.

formalism and interconnected through a 16-state model of GI channel gating (16SM). We demonstrate that during the spread of excitation, a delay between action potentials (APs) creates a bipolar V_i spike of approximately ± 100 mV, causing relatively small decay of g_i , which can accumulate into significant g_i decays during bursting activity of neurons. Also, we demonstrate that very low g_i allows for synchronization of a network composed of neurons exhibiting different intrinsic firing frequencies. Furthermore, we show that a relatively small heterogeneity in I-V rectification of GIs creates conditions for unidirectional AP propagation, leading to reverberation of excitation, which, as proposed (Lorente de Nó, 1933; Hebb, 1950; Tegnér et al., 2002; Constantinidis and Wang, 2004; Wang et al., 2004, 2011), can serve as a form of short-term memory and can mediate consolidation of short-term memory into longterm memory.

MATERIALS AND METHODS

Model of the neuronal network

We linked up to several hundred cells into a 2-D cluster, each exhibiting excitability described using H-H equations (Hodgkin and Huxley, 1952). Each cell in the cluster communicated with neighboring cells through GJs. Junctional current (I_j) and g_j were simulated using stochastic 16SM (S16SM) and Markov chain 16SM (MC16SM). We used the sets of 16SM parameters, which are presented in Tables 1 and 2. All models were implemented in MATLAB.

H-H model

We have modified the original H-H model (Hodgkin and Huxley, 1952) by adding I_p described by the following system of ordinary differential equations:

$$\begin{cases} I_{m} = I_{ext} + C_{m} \frac{dV_{m}}{dt} + g_{K} n^{4} \left(V_{m} - V_{K}\right) + g_{Na} m^{3} h\left(V_{m} - V_{Na}\right) + g_{l}\left(V_{m} - V_{l}\right) + I_{j}; \\ \frac{dn}{dt} = \alpha_{n}\left(V_{m}\right) \cdot (1 - n) - \beta_{n}\left(V_{m}\right) \cdot n; \\ \frac{dm}{dt} = \alpha_{m}\left(V_{m}\right) \cdot (1 - m) - \beta_{m}\left(V_{m}\right) \cdot m; \\ \frac{dh}{dt} = \alpha_{h}\left(V_{m}\right) \cdot (1 - h) - \beta_{h}\left(V_{m}\right) \cdot h. \end{cases}$$

Here, I_m is the transmembrane current per unit area, I_{ext} is external stimulus current, V_m is membrane potential, and C_m is the membrane capacitance per unit area; V_K , V_{Na} , and V_I are the potassium, sodium, and leak reversal potentials, respectively; g_K , g_{Na} , and g_I are the maximum values of potassium, sodium, and leak conductances per unit area, respectively; n, m, and h are variables ($0 \le n$, m, $h \le 1$) associated with potassium channel activation, sodium channel activation, and sodium channel inactivation, respectively; and α_i and β_i are rate constants for the respective ion channels.

The membrane capacity C_m was chosen as $1 \, \mu F/cm^2$. The corrected values of reversal potentials were chosen as $V_K = -12$, $V_{Na} = 115$, and $V_l = 10.6$ mV, whereas conductances were chosen as $g_K = 36$, $g_{Na} = 120$, and $g_l = 0.3$ mS/cm² (Hodgkin and Huxley, 1952). The functions α_i and β_i were as follows:

TABLE 1
Set of parameters of MC16SM used for simulation of multicellular networks

Gate/Parameter	A	V_0	γ_{open}	$\gamma_{\it closed}$	R_{open}	R_{closed}	P_t	П
	mV^{-1}	mV	pS	pS	mV	mV		
Fast gate	0.15	40	24	3	10,000	10,000	0.00005	-1
Slow gate	0.15	40	24	0	10,000	-	0.00005	-1

The set of parameters of an MC16SM used for simulation of multicellular networks interconnected through electrical synapses formed of GJ channels resembling Cx36 and to assemble Figs. 3 B, 4 (E–G), 5, 6, 7, and 8. In search of minimum g_j necessary for synchronization and signal transfer of APs in 1-D and 2-D clusters of neurons ($g_{j,min-synch}$ and $g_{j,min-transfer}$ Fig. 5), we varied the number of GJ channels forming electrical synapses.

$$\alpha_n(V_m) = \frac{0.1 - 0.01 \cdot V_m}{e^{(1 - 0.1 \cdot V_m)} - 1};$$

$$\alpha_m(V_m) = \frac{2.5 - 0.1 \cdot V_m}{e^{(2.5 - 0.1 \cdot V_m)} - 1};$$

$$\alpha_h(V_m) = 0.07 \cdot e^{\left(-\frac{V_m}{20}\right)};$$

$$\beta_n(V_m) = 0.125 \cdot e^{\left(-\frac{V_m}{80}\right)};$$

$$\beta_m(V_m) = 4 \cdot e^{\left(-\frac{V_m}{18}\right)};$$

$$\beta_h(V_m) = \frac{1}{e^{(3-0.1\cdot V_m)} + 1}.$$

We used Euler's method for the numerical solution of H-H model equations, which was implemented in MATLAB. A time step of 0.01 ms was used in most numerical experiments.

S16SM

In an S16SM (Paulauskas et al., 2012), each of four gates is characterized by gating properties and the unitary conductance of the open (o) and closed (c) states (Fig. 1 C). We have used an S16SM approach to describe the operation of each gate, allowing a simulation of I_j and g_j changes over time. This model is available online at http://connexons.aecom.yu.edu/Applet.htm, and its application in analyzing gating of GJs under normal and pathologic conditions was reported in Palacios-Prado et al. (2009, 2010) and Skeberdis et al. (2011).

In general, the model defines the probability of an individual gate to remain in the same state or to change its state for any given discrete time interval (Δt) and V_j . Closing one gate changes voltage across the other three gates in series, which will affect their probability of changing the state over the next Δt . The

transition probabilities between open and closed states $p_{o \to c}$ and $p_{c \to o}$ or probabilities to remain in the same state $(p_{o \to o}$ and $p_{c \to c})$ are given by

$$p_0 \rightarrow c(K, P_t) = \frac{P_t \cdot K}{1 + K},$$

$$p_{o \to o}(K, P_t) = 1 - p_{o \to c}(K, P_t),$$

$$p_{c \to o}(K, P_t) = \frac{P_t}{1+K},$$

and

$$p_{c \to c}(K, P_t) = 1 - p_{c \to o}(K, P_t),$$

where P_t adjusts probability of transitions during a discrete time interval, Δt , to equilibrate simulated and experimental times (Paulauskas et al., 2009, 2012). K is the equilibrium constant of slow/fast gate, determined as follows: $K_{S/F,o\leftrightarrow c} = e^{A_{S/F}\left(-\Pi \cdot V_{S/F} \cdot V_{S/F,o}\right)}$ (Chen-Izu et al., 2001). Here, $A_{S/F}$ characterizes sensitivity to voltage, $V_{S/E,o}$ is voltage at which $K_{S,o\leftrightarrow c}$ or $K_{S,o\leftrightarrow rs}$ is equal to 1, and Π is a gating polarity (+1 or -1). $V_{S/F}$ is voltage across fast/slow gate.

There is a solid body of evidence demonstrating I-V rectification of open and residual states of the GJ channel and an unapposed hemichannel (DeVries and Schwartz, 1992; Trexler et al., 1996; Oh et al., 1999; Bukauskas et al., 2002a; Kronengold et al., 2003; Valiunas et al., 2004; Tong and Ebihara, 2006; Rackauskas et al., 2007). We assumed that $\gamma_{S,open}$, $\gamma_{F,open}$, and $\gamma_{E,res}$ rectify in accordance with the exponential function as proposed in Vogel and Weingart (1998): $\gamma_{F,open} = \gamma_{F,open,0} \cdot e^{V_F/R_{F,open}}$, $\gamma_{F,res} = \gamma_{F,res,0} \cdot e^{V_F/R_{F,open}}$, $\gamma_{F,res} = \gamma_{F,res,0} \cdot e^{V_F/R_{F,open}}$, and $\gamma_{S,open} = \gamma_{S,open,0} \cdot e^{V_S/R_{S,open}}$, where $\gamma_{S,open} = \gamma_{S,open,0} \cdot e^{V_S/R_{S,open}}$, and $\gamma_{S,open} = \gamma_{S,open,0} \cdot e^{V_S/R_{S,open}}$, where $\gamma_{F,open,0}$ and $\gamma_{E,res,0}$ are $\gamma_{E,open}$ at $V_F = 0$, whereas $\gamma_{S,open,0}$ is $\gamma_{E,open}$ at $V_S = 0$. $R_{E,open}$, $R_{E,res}$, and $R_{S,open}$ are rectification coefficients of the open/residual states and fast/slow gates, respectively.

Rectification of $\gamma_{F,open}$, $\gamma_{F,res}$, and $\gamma_{S,open}$ does not allow for the evaluation of V_F and V_S in one step and necessitates the use of an iterative procedure to estimate the conductance of the GJ channel. In brief, initially we know the states of each gate, which allows for the estimation of V_F and V_S without accounting for rectification:

TABLE 2
Set of parameters of S16SM and MC16SM used for simulation of multicellular networks

Gate/Parameter	A	V_0	γ_{open}	γ_{closed}	R_{open}	$R_{\rm closed}$	P_t	П
	mV^{-1}	mV	pS	pS	mV	mV		
Fast gate	0.15	10	120	10	10,000	10,000	0.00005	-1
Slow gate	0.15	10	120	0	10,000	-	0.00005	-1

The set of parameters of an S16SM and an MC16SM used for simulation of multicellular networks interconnected through electrical synapses formed of GJ channels resembling Cx45 and to assemble Figs. 2, 3 (C and D), and 4 (B–D, F, and G).

$$V_{F,A} = \frac{V_j \cdot \gamma_j}{\gamma_{F,A}},$$

$$V_{S,A} = \frac{V_j \cdot \gamma_j}{\gamma_{S,A}},$$

$$V_{S,B} = \frac{V_j \cdot \gamma_j}{\gamma_{S,B}},$$

and

$$V_{F,B} = \frac{V_j \cdot \gamma_j}{\gamma_{F,B}}.$$

Then, we recalculate conductances of gates accounting for rectification and reevaluate a new set of V_F and V_S . We repeat the last cycle and at the nth iterative step evaluate conductance of the GJ channel $(\gamma_{j,n})$ as well as the difference, $\Delta \gamma_{j,n} = \gamma_{j,n} - \gamma_{j,n-1}$ for convergence testing. The value of $\gamma_{j,n}$ is given by

$$\gamma_{j,n} = \frac{1}{\left(\frac{1}{\gamma_{\text{F,A}}} + \frac{1}{\gamma_{\text{S,A}}} + \frac{1}{\gamma_{\text{S,B}}} + \frac{1}{\gamma_{\text{F,B}}}\right)}.$$

The iterative procedure is stopped once the tolerance criterion $\Delta \gamma_{j,n} < (\gamma_{j,n-1}/1000)$ is reached. The final values of V_F and V_S allow for the evaluation of possible changes in the state of each gate, as well as estimation of voltages across all four gates, the sum of which should be equal to V_p i.e., $V_j = V_{EA} + V_{S,A} + V_{EB} + V_{S,B}$.

This information is transferred to the next discrete time interval and the process is repeated. In >99% of calculations, the number of iterations was four to seven. Once the effect of I-V rectification on the unitary conductance of each GJ channel $\gamma_{j,i}$ of the electrical synapse composed of m channels is evaluated, then g_i is estimated from

$$g_j = \sum_{i=1}^m \gamma_{j,i}$$
.

MC16SM

To accelerate the simulation and reduce noise, we developed an MC16SM by transforming an S16SM. Instead of evaluating gating of each individual GJ channel, we calculated changes over time of averaged probabilities for each of four gates to be open or closed depending on V_i by using a Markov chain approach. Earlier, we used stationary/steady-state probabilities of Markov chain to model GJ voltage gating (Sakalauskaite et al., 2011; Snipas et al., 2015). However, a steady-state approach is not suitable in this case, because modeling of neuronal networks requires evaluation of dynamic changes in g_i . Thus, we used transitive rather than steady-state probabilities. In doing so, we used a recursive relation, $p^n = p^{n-1} \cdot P$, to calculate the transitive probability vector pⁿ at a discrete time moment, t_n , for each of 16 states, where P denotes the transition probability matrix of a discrete-time Markov chain. Each state s; can be expressed as a 4-tuple, $s_i = (s_{F,A}; s_{S,A}; s_{S,B}; s_{F,B})$, where each component denotes the state—open (o) or closed (c)—of the respective gate in the GJ channel. Thus, the model consists of 16 states, which can be numbered in lexicographical order as follows: $s_1 = (o;o;o;o)$; $s_2 = (o;o;o;c); s_3 = (o;o;c;o); s_4 = (o;o;c;c); s_5 = (o;c;o;o); s_6 = (o;c;o;c);$ $s_7 = (o;c;c;o); s_8 = (o;c;c;c); s_9 = (c;o;o;o); s_{10} = (c;o;o;c); s_{11} =$ $(c;o;c;o); s_{12} = (c;o;c;c); s_{13} = (c;c;o;o); s_{14} = (c;c;o;c); s_{15} = (c;c;c;o);$ and $s_{16} = (c;c;c;c)$.

The transition probabilities among 16 states can be expressed by using the same transition probabilities $p_{o\to c}$ and $p_{c\to o}$ of singular $o\!\!\leftarrow\!\!>c$ transitions, as in S16SM. For example, transition probability from $s_4 = (o,o,c,c)$ to $s_6 = (o,c,o,c)$, which we denote as $p_{ooc-occoc}$ can be estimated as follows: $p_{ooc-occoc} = (1 - p_{o\to c}) \cdot p_{o\to c} \cdot p_{c\to o} \cdot (1 - p_{c\to o})$.

Thus, all basic parameters of the model necessary for building a transition probability matrix P are the same as in the S16SM model, and the same equations are used to estimate K, evaluate I-V rectification, and calculate γ_j . However, because voltage across each gate depends on the state s_j , i.e., $V_F = V_F(s_j)$ and $V_S = V_S(s_j)$, then γ_j must also be evaluated at each state, i.e., $\gamma_j = \gamma_j(s_j)$. Once the transition probability matrix P is formed and the probability vector \mathbf{p}^n is estimated, then the expected value of junctional conductance g_i is estimated as

$$g_j = \sum_i p_i \cdot \gamma(s_i).$$

Fig. 2 shows I_j (B) and g_j (C) traces generated in response to a V_j step of -60 mV (A) using an S16SM (red traces) and an MC16SM (blue traces).

Online supplemental material

Fig. S1 supplements Fig. 4 C. Fig. S2 supplements Fig. 5. Figs. S3–S6 are snapshots of Fig. 8 and Videos 1–4 and provide explanations of conditions under which these videos were recorded. A more detailed description of 16SM is presented in the supplemental materials and methods. Online supplemental material is available at http://www.jgp.org/cgi/content/full/jgp.201511488/DC1.

RESULTS

Physiology of fast and slow gates

The demonstration of fast and slow gates (Bukauskas and Verselis, 2004) required consideration of four gates in series, which resulted in the development of an S16SM of gating (Paulauskas et al., 2012). The initial hypothesis of fast and slow gating mechanisms was based on recordings of de novo GJ channel formation observed after providing two patched insect cells (Aedes albopictus, clone C6/36) in contact (Bukauskas and Weingart, 1993, 1994). Based on these data, it was concluded that each hemichannel of the GI channel possesses a fast gate controlled by V_i that closes the channel from the open state with conductance $\gamma_{p,o}$ to a substate or residual state with conductance $\gamma_{i,res}$ and a slow gate that operates between an open state with conductance $\gamma_{S,open}$ and a fully closed state with conductance $\gamma_{S,closed} = 0$ (Fig. 1 A; Bukauskas and Weingart, 1994). Furthermore, gating of GIs to the substate were reported in mammalian cells expressing different Cx isoforms (Moreno et al., 1994; Veenstra et al., 1994; Bukauskas et al., 1995; Bukauskas and Peracchia, 1997).

Furthermore, there is a solid body of evidence demonstrating I-V rectification of open and residual states of the single GJ channel (Bukauskas et al., 2002a; Rackauskas et al., 2007) and undocked/unapposed hemichannels (DeVries and Schwartz, 1992; Trexler et al., 1996; Oh et al., 1999; Kronengold et al., 2003; Valiunas et al., 2004; Tong and Ebihara, 2006). I-V rectification of gates is

typically reflected in the nonlinear instantaneous g_i ($g_{i,inst}$) dependence on V_i measured at the very beginning of applied V_i steps when V_i gating is not yet activated. Homotypic GJ channels, which exhibit oppositely oriented near-exponential relationships of $\gamma_{F,open}$ or $\gamma_{S,open}$ over V_i in aHCs, demonstrate a relatively small $g_{i,inst}$ dependence on V_i , as shown in Fig. 7 of Paulauskas et al. (2009). However, if cells express different Cx isoforms and form heterotypic GJ channels or are exposed to asymmetric conditions in ionic composition or phosphorylation, which can differently affect I-V rectification of fast and/or slow gates residing in aHCs, then an asymmetry of I-V rectification of GJ channels can be well expressed, causing unidirectional signal transfer and reverberation of excitation in neuronal networks, as we demonstrate later in Figs. 7 and 8.

Simulation of signal transfer through electrical synapses

Studies of electrical cell-cell coupling in brain slices are most often performed by injecting a pulse of constant hyperpolarizing current into one cell and measuring the electrotonic response in a neighboring cell. Initially, we simulated electrotonic signal transfer between two cells connected through soma-somatic junctions (Fig. 3 A). Cell 1 was injected with an external current (I_{ext}) under current clamp conditions, and the changes in transmembrane voltages were estimated in cell 1 $(V_{m,1})$ and cell 2 $(V_{m,2})$. Fig. 3 B shows that at $g_i = 0.2$ nS, electrotonic responses in cell 1 (V_1) and cell 2 (V_2) reached steady states after \sim 30 ms. The ratio between V_2 and V_1 is named as a coupling coefficient, $K_{12} = V_2/V_1$. The bottom plot in Fig. 3 A shows the K_{12} - g_i relationship simulated for soma-somatic GJs; the gray circle shows averaged K_{12} (~ 0.15) and g_i $(\sim 0.2 \text{ nS})$ values measured in rat cerebellar cortex basket cells (Alcami and Marty, 2013). However, for dendro-dendritic GJs located relatively distantly from somas (more than ~100 µm), an influence of axial resistance of the dendrites (R_d in Fig. S1 B and supplemental materials and methods) should be accounted for. Our preliminary data demonstrate that g_i values are increasingly undervalued with an increase in the distance of electrical synapse from somas of communicating neurons (unpublished data).

In testing whether the strength of electrical synapses can cause gating, we initially assumed that cells are connected through the relatively highly V_7 sensitive Cx45, which, like Cx36, is expressed in neurons, but to a lesser degree (von Maltzahn et al., 2004; Chapman et al., 2013). Fig. 3 C shows that an $I_{\rm ext}$ of -18 pA caused changes in $V_{m,1}$ and $V_{m,2}$, resulting in a V_j of ~ 30 mV; simulation was performed using MC16SM. The g_j trace demonstrates that g_j decayed, and it took ~ 600 ms to reach a steady state at $\sim 50\%$ of the initial g_j . With the decrease in g_j , $V_{m,1}$ increased and $V_{m,2}$ decreased (Fig. 3 C, left inset in V_m time plot), thus causing V_j to rise, which accelerated a decay in g_j . Furthermore, after an $I_{\rm ext}$ step, the AP developed in cell 1 and was transmitted to cell 2

with a \sim 2-ms delay that generated a bipolar V_j pulse (Fig. 3 C, inset on V_j time plot), resulting in a small decrease in g_j (arrow in the inset of g_j time plot). Assuming that GJs are formed of the less V_j -sensitive Cx36 ($V_{E,o}$ and $V_{S,o}$ were 40 mV instead of 10 mV for Cx45; Bukauskas et al., 2002b; González et al., 2007; Marandykina et al., 2013), then the g_j decrease was \sim 10-fold lower (unpublished data). Gating parameters of Cx36 and Cx45 are shown in Tables 1 and 2.

Fig. 3 D shows data simulated using S16SM instead of MC16SM; parameters of gates were the same as in Fig. 3 C. It was assumed that the electrical synapse contained 10 GJ channels with a single-channel conductance of 25 pS. This revealed stepwise rather than smooth changes in g_j . It is notable that the unitary stepwise changes in g_j resulted in slow changes in $V_{m,1}$ and $V_{m,2}$ (Fig. 3 D, left inset in g_j time plot).

To assess the extent to which the V_j values that develop during spiking activity can affect g_j , we exposed cell 1 of the cell pair to $I_{\rm ext}$ of +15 pA (Fig. 4 A), which caused a burst of APs at 63 Hz in cell 1 (Fig. 4 B, red trace). Then, excitation was transferred to cell 2 (Fig. 4 B, blue trace) with a \sim 2-ms delay (Fig. 4 B, inset, \leftrightarrow). In this simulation, $V_{F,o} = V_{S,o} = 10$ mV, which roughly corresponds to Cx45. Fig. 4 C shows repeated V_j values arising mainly during the phase shift between APs in neighboring cells, which we term $V_{j,AP}$. The amplitude of the $V_{j,AP}$ spike can reach approximately ± 100 mV, which caused a \sim 2% decrease in g_j (Fig. 4 D, inset on g_j trace). During bursting activity of neurons, small reductions in g_j accumulate,

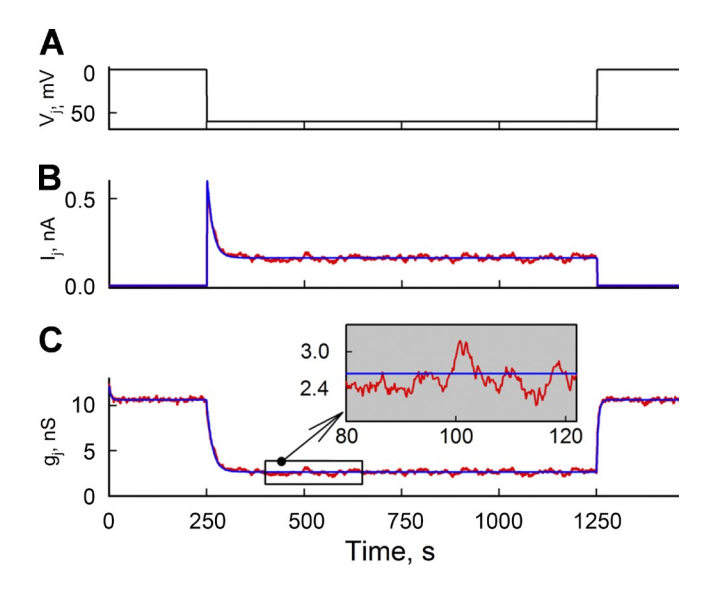


Figure 2. Comparison of I_j and g_j time plots simulated using an S16SM and an MC16SM. (A) V_j step of -60 mV applied to one cell of the cell pair. Both cells were voltage clamped. (B) I_j time plots obtained simulating a junction composed of 500 channels using an S16SM (red) and an MC16SM (blue). (C) g_j time plots obtained from the ratio I_j/V_j . g_j values evaluated using MC16SM (blue) reflect averaged changes of g_j values obtained using S16SM (red) and are virtually free of noise (inset).

giving a \sim 28% decrease in g_j at the steady state (Fig. 4 D). However, Fig. S1 A (see also supplemental materials and methods) shows that at higher g_j values (2 instead of 0.36 nS), the phase shift between APs in neighboring cells decreases, resulting in substantially shorter and smaller-amplitude $V_{j,AP}$ spikes. Consequently, this caused a \sim 30% smaller drop in g_j than that shown in Fig. 4 D.

At $V_{F,o} = V_{S,o} = 40$ mV, which resembles Cx36 properties, a decrease in g_j during one $V_{j,AP}$ spike was $\sim 0.35\%$, which accumulated during bursting activity, resulting in a $\sim 2.5\%$ decrease in g_j (Fig. 4 E). Fig. 4 F shows that a

greater decrease of g_j in cells expressing Cx45 correlates with a larger delay of AP transfer than in Cx36-expressing cells. Fig. 4 G shows how the reduction of g_j depends on $V_{F,o}$ and $V_{S,o}$, which roughly replicate gating of different Cxs at $I_{\rm ext}$ = +15 pA (squares; spiking activity is present). Thus, g_j can decrease \sim 30% in highly V_j -sensitive Cx45 or Cx57, whereas for less V_j -sensitive Cxs, e.g., Cx36 or Cx26, the decrease in g_j was much smaller. Even though electrical synapses are formed preferentially of Cx36 GJs exhibiting low V_j sensitivity under normal conditions, their sensitivity to V_i increases significantly when

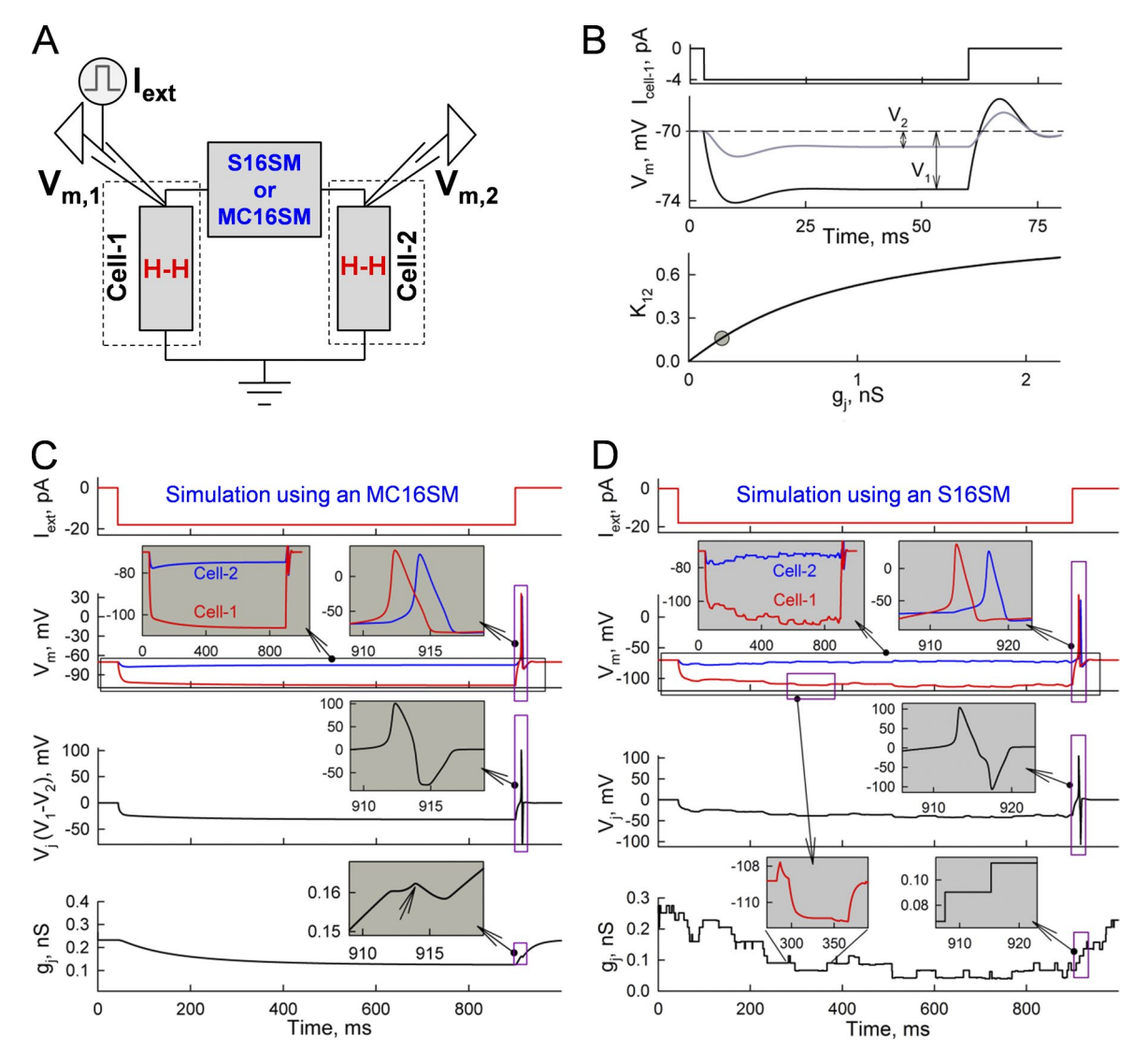


Figure 3. Simulation of cell–cell coupling through soma-somatic GJs. (A) The scheme illustrates two cells, each exhibiting an excitability described by H-H formalism and communicating through GJs operating according with an S16SM or an MC16SM. The left electrode was used to inject current (I_{ext}) under current clamp mode and measure transmembrane voltage in cell 1 ($V_{m,1}$). The right electrode was used to record transmembrane voltage in cell 2 ($V_{m,2}$). (B) Electrotonic responses evoked in cell 1 (V_1) and cell 2 (V_2) by an I_{ext} step of -4 pA. Simulations were performed using an MC16SM. (C) Simulation of changes in $V_{m,1}$, $V_{m,2}$, and g_j caused by gating of GJs formed of the Cx exhibiting properties similar to Cx45, in response to an I_{ext} step of -18 pA. Simulation was performed using an MC16SM. The left inset in the V_m time plot shows that before reaching a steady state, $V_{m,1}$ increases and $V_{m,2}$ decays, resulting in an increase of V_j and V_j gating. Phase differences between APs arising at the end of the I_{ext} step caused a bipolar V_j spike (inset in V_j time plot) and, consequently, a small decay of g_j (inset in g_j time plot) caused by V_j gating. (D) Simulation as in A, but performed using an S16SM instead of an MC16SM and assuming that the junction contains 10 GJ channels.

intracellular Mg^{2+} ($[Mg^{2+}]_i$) is elevated to 5 mM (Palacios-Prado et al., 2013), which would lead to larger reductions in g_j during bursting activity of neurons. Also, a robust increase in sensitivity to V_j was demonstrated for Cx45 and Cx57 during acidification (Palacios-Prado et al., 2009). Hence, the decrease in g_j that occurs during bursting activity depends not only on Cx type but also on the surrounding conditions influencing the functional state of the cell.

To examine whether $V_{j,AP}$ spikes and changes in g_j are different for dendro-dendritic junctions, we simulated the cell pair with a principal electrical scheme as shown in Fig. S1 B and the supplemental materials and methods.

Parameters of fast and slow gates as well as the value of g_j were identical to those of the soma-somatic junction. Fig. S1 C shows that $V_{j,AP}$ spikes obtained for soma-somatic (red) and dendro-dendritic (green) junctions are similar in amplitude and duration, whereas both cause g_j decay similar to that shown in Fig. 4 D.

Role of electrical synapses in synchrony of neuronal networks Synchronization of neuronal networks can be achieved through chemical (Brunel and Hakim, 1999; Juang and Liang, 2014) as well as electrical (Hormuzdi et al., 2004) synapses. It is known that neurons coupled through electrical synapses can exhibit synchronous

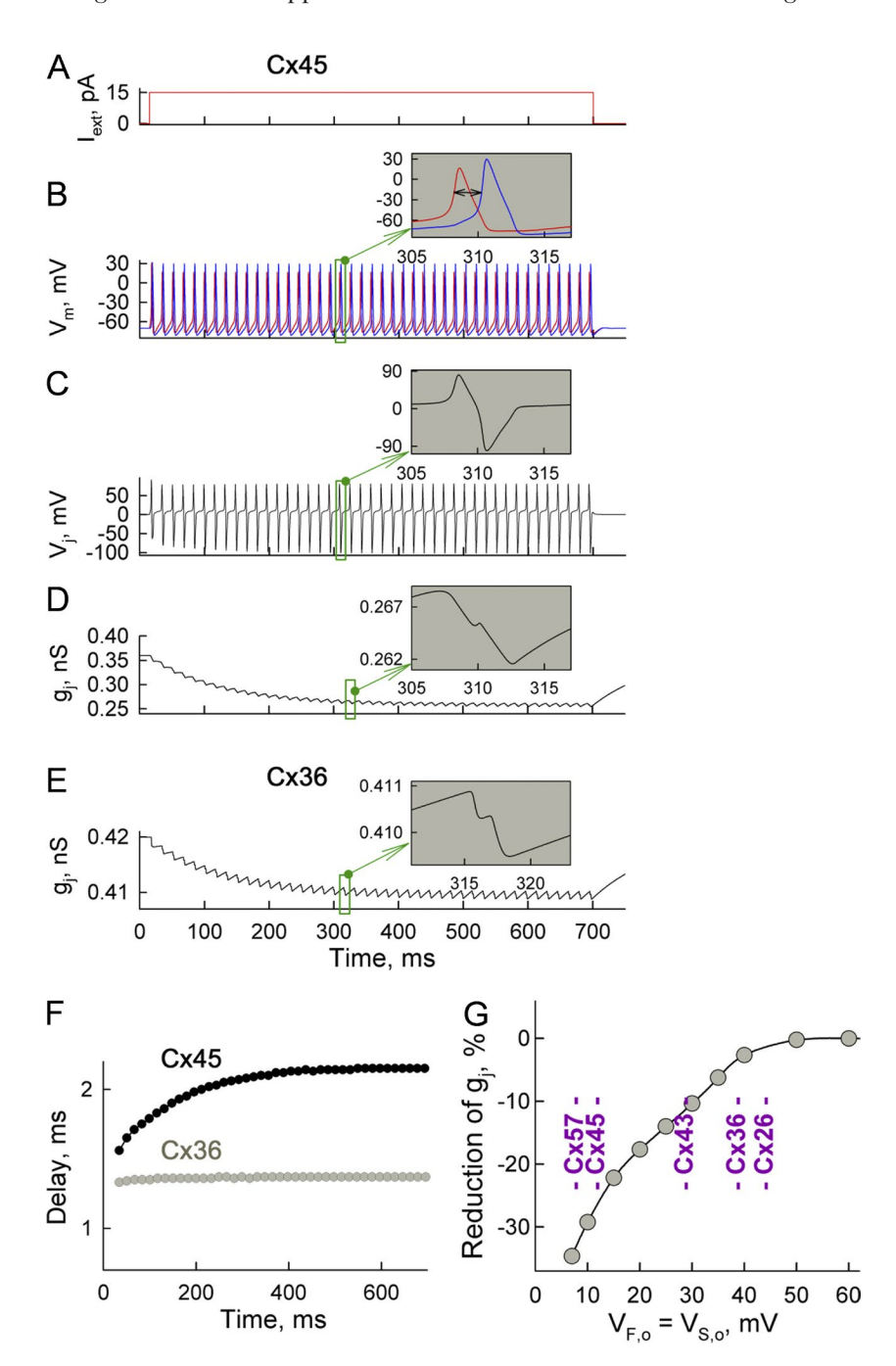


Figure 4. Changes of GIC in the pair of neurons exhibiting bursting activity. (A-D) Demonstration of changes in V_m , V_j , and g_j over time for GJs formed of hypothetical Cx45 in response to an I_{ext} step of 15 pA. (B) Burst of APs evoked in cell 1 (red) and then transferred to cell 2 (blue). Inset shows that the delay between APs was \sim 2 ms. (C) Transjunctional voltage was defined as $V_i = V_{m,cell 1} - V_{m,cell 2}$; inset shows bipolar V_i spikes arising because of a phase difference between APs. (D) Decay of g_i during the I_{ext} step. (E) Decay of g_i of GJs formed of connexin exhibiting gating properties resembling those of Cx36. (F) Delay of AP transfer from cell 1 to cell 2 increased by $\sim 38\%$ in cells expressing Cx45 and at a much smaller level for cells expressing Cx36. (G) Predicted reduction in g_i during I_{ext} steps of 15 pA in the cell pair expressing various Cx isoforms. All simulations were performed using an MC16SM.

spiking activity while being separated by several hundred micrometers (Alcami and Marty, 2013). Otherwise, it is well established that electrical cell-cell coupling between neurons is relatively weak. In neuronal networks connected through dendro-dendritic GJs, g_i values are <1 nS (~ 0.13 nS in Vervaeke et al. [2010], 0.02-0.2 nS in Venance et al. [2004], and 0.13-1.0 nS in Devor and Yarom [2002]). Higher values of g_i were reported for soma-somatic junctions (mean ~2.1 nS between low-threshold spiking thalamocortical neurons in Gibson et al. [1999] and ~6 nS in clusters of mesencephalic trigeminal nucleus neurons in Curti et al. [2012]). Relatively small g_i values of electrical synapses are most likely caused by a very small single-channel conductance of Cx36 GJ channels (~6 pS; Moreno et al., 2005) and the small size of junctional plaques (JPs; Rash et al., 2013).

We examined a minimum g_j required to achieve phase synchronization/lock in a cluster of two or more cells $(g_{j,min-synchr})$, each of which exhibits spontaneous activity but differs in firing rates. Fig. 5 A (b) shows that at $g_j = 0$, cell 1 exposed to $I_{\rm ext}$ of 35 pA exhibited APs at 95 Hz, and cell 2 exposed to $I_{\rm ext}$ of 12 pA exhibited APs at 65 Hz. When g_j was increased and reached 0.26 nS, cells exhibited phase-locked oscillations (Fig. 5 A, c) at an intermediate frequency of 85 Hz. Fig. 5 A (a) shows $g_{j,min-synchr}$ dependence on the maximum difference in firing rates (Δ FR) among cells in the 2-D clusters; random distributions of firing rates were created by using different $I_{\rm ext}$ values. For each 2-D cluster consisting of $n \times n$ cells, five different numerical experiments were performed.

Parameters of an MC16SM were selected assuming that GJs are formed of Cx36 (Table 1). The central cell of the cluster was exposed to the highest $I_{\rm ext}$ value, whereas values between minimum and maximum $I_{\rm ext}$ and assignments to other cells were selected randomly. Fig. 5 B shows that $g_{j,min-synchr}$ approaches zero at small Δ FR and increases as Δ FR rises. It also demonstrates that averaged values of $g_{j,min-synchr}$ tend to be higher for bigger clusters but approach steady state at the cluster size of \sim 7 × 7. Also, $g_{j,min-synchr}$ values of 1-D or cable-like (1 × n) clusters were at least \sim 30% higher than those of 2-D clusters.

At $g_i = 0$, if cell 1 of the cell pair is exposed to 2-ms-long depolarizing pulses of 30 pA at 70 Hz, then it exhibits regular firing activity while other cells remain silent. When g_i was increased and reached 0.1625 nS, cell 2 responded with an AP to every AP in cell 1. Summary of Fig. 5 C shows that the minimum g_i necessary for one-toone AP transfer $(g_{j,min-transf})$ in the cell pair increases with rising frequency of I_{ext} pulses. Also, the values of g_{j,min-transf} increased as the size of the 2-D cluster increased from 2×2 to 7×7 . In all experiments, the cell exposed to repeated stimulation was located maximally close to the center of the cluster. There was a clear convergence to a steady state when the size of the cluster reached 4×4 . Furthermore, there is well-expressed decay of a cutoff of frequency from \sim 95 Hz for the cell pair to \sim 70 Hz for 4×4 to 7×7 clusters with an increase in size of the cluster. Also, at \sim 50 Hz, there is a well-expressed minimum of $g_{i,min-synchr}$ for all sizes of clusters, which is most likely related to the enhanced amplitude (~8%) of APs initiated at the period of excitation of 20 ms.

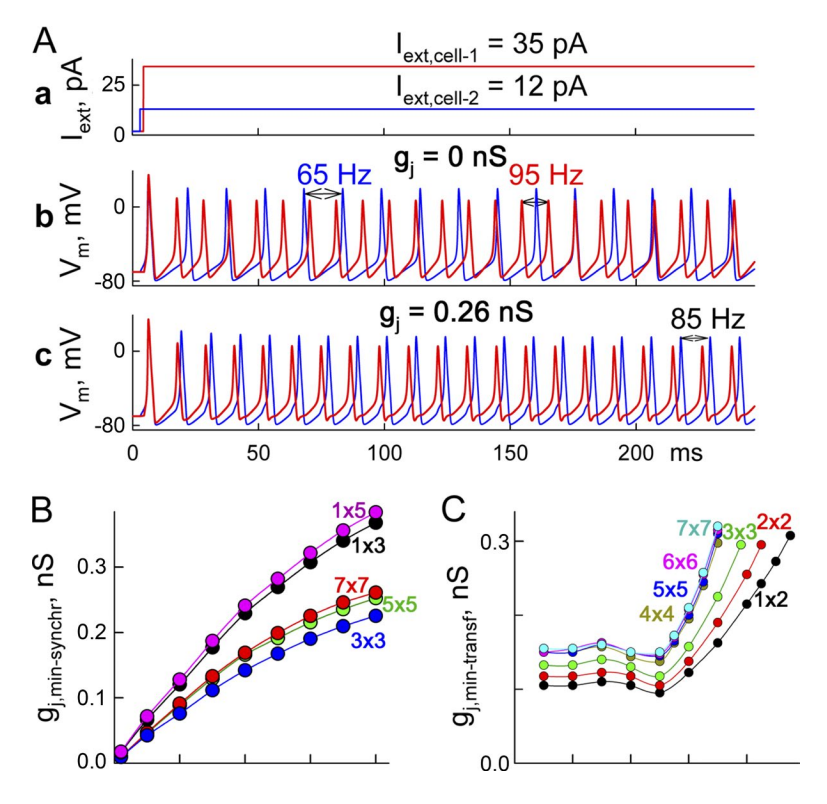


Figure 5. Synchronization of neuronal clusters. (A and B) Minimum values of g_i necessary for synchronization of neuronal networks $(g_{j,min-synchr})$. (A) Repeated APs in cell 1 (red) and cell 2 (blue; b and c) evoked by long depolarizing current pulses shown in a. At $g_i = 0$, cells exhibited repeated spiking activity at 65 and 95 Hz (b) and $g_i = 0.26$ nS (c). (B) Summarized data of $g_{j,min-synchr}$ values in 1-D and 2-D clusters of different sizes depending on differences in their firing rates of neurons, ΔFR . (C) Summary of the minimum g_i necessary for AP transfer between neurons $(g_{j,min-transf})$ depending on frequency of APs caused by repeated 2-ms-long I_{ext} steps of 30 pA. Values of $g_{i,min-transf}$ were evaluated in the cell pair (1×2) and 2-D clusters ranging from 2×2 to 7×7 .

To evaluate how V_j gating affects synchronization of neuronal networks, we examined a network interconnected through (a) constant resistors, (b) GJs formed of low- V_J -sensitivity Cx36, and (c) GJs interconnected through high- V_J -sensitivity Cx45. Fig. S2 shows that the difference in $g_{min,synch}$ between Cx36 and the constant resistors is negligible (<2%). However, for Cx45, $g_{min,synch}$ was more than two times higher. We expect that a similar increase in $g_{min,synch}$ can occur for Cx36 under intracellular hypermagnesemia (Palacios-Prado et al., 2013, 2014), which increases V_T -sensitive gating of Cx36.

Unidirectional AP transfer between cells connected through GJs exhibiting I-V rectification

Cells, despite well-expressed homeostasis, differ in pH, electrolytic balance, phosphorylation, etc., which may cause an asymmetry in cell-to-cell signaling. Asymmetry in GJC was observed in approximately one third of cases between striatal output neurons (Venance et al., 2004) and between neurons in the inferior olive nucleus (Devor and Yarom, 2002). Recently, we reported that asymmetry in $[Mg^{2+}]_i$ leads to rectification of $g_{j,inst}$ (Palacios-Prado et al., 2014). To explore how I-V rectification can affect signal transfer between cells, we simulated AP transfer in three linearly arranged cells connected through an MC16SM (Fig. 6 A). We assumed that the junction between cells 1 and 2 exhibited well-expressed I-V rectification as shown in the red $g_{i,1-2}$ – V_i plot (Fig. 6 B), whereas the junction between cells 2 and 3 was not rectifying (blue $g_{j,2-3}$ line); I-V rectification coefficients of GJs were equal to 150 and 10,000 mV, respectively. Cell 2 was excited by a 50-pA pulse 1 ms in duration. This caused an AP in cell 2 (Fig. 6 C). Difference in V_m between cells 1 and 2 resulted in short-lasting V_i with an amplitude reaching ~ 100 mV. The orientation of I-V rectification was such that at positivity on the cell 2 side, $g_{i,1-2}$ decreased (red trace), causing a block of AP transfer to cell 1 (green V_m trace), whereas excitations were transferred to cell 3. Stimulation of cell 1 (Fig. 6 D) induced an AP during which cell 1 became more positive than cell 2 and, because of I-V rectification and oppositely oriented V_i , $g_{i,1-2}$ increased, which facilitated AP transfer to cell 2 and onto cell 3. Thus, relatively weak I-V rectification of GJs can lead to unidirectional signal transfer between neurons.

Reverberation of excitation in a cluster of cells connected through electrical synapses

It is well established that unidirectional signal transfer or an interruption/brake of the wave of excitation can initiate reverberation or reentry, causing heart fibrillation (Davidenko et al., 1995). Here, we present data demonstrating formation of reverberation in a cluster of nine neurons connected through electrical synapses (Fig. 7). Assuming that GJs do not exhibit I-V rectification and g_i values of electrical synapses are distributed

randomly in a range of 0.175–0.2 nS, then an AP evoked in cell 1 spreads through the cluster and terminates (Fig. 7 B). When I-V rectification was ascribed between cells 1 and 4 and between cells 2 and 5, leaving other GJs lacking rectification, then an $I_{\rm ext}$ pulse of 25 pA (Fig. 7 C, a) initiated an AP in cell 1 that was transmitted to cell 2, but not to cell 4 (Fig. 7 C, d). Consequently, the excitation spread along the yellow circle (Fig. 7 A). After reexcitation of cell 1, the process repeated many times. Interestingly, cell 5 exhibited only low-amplitude

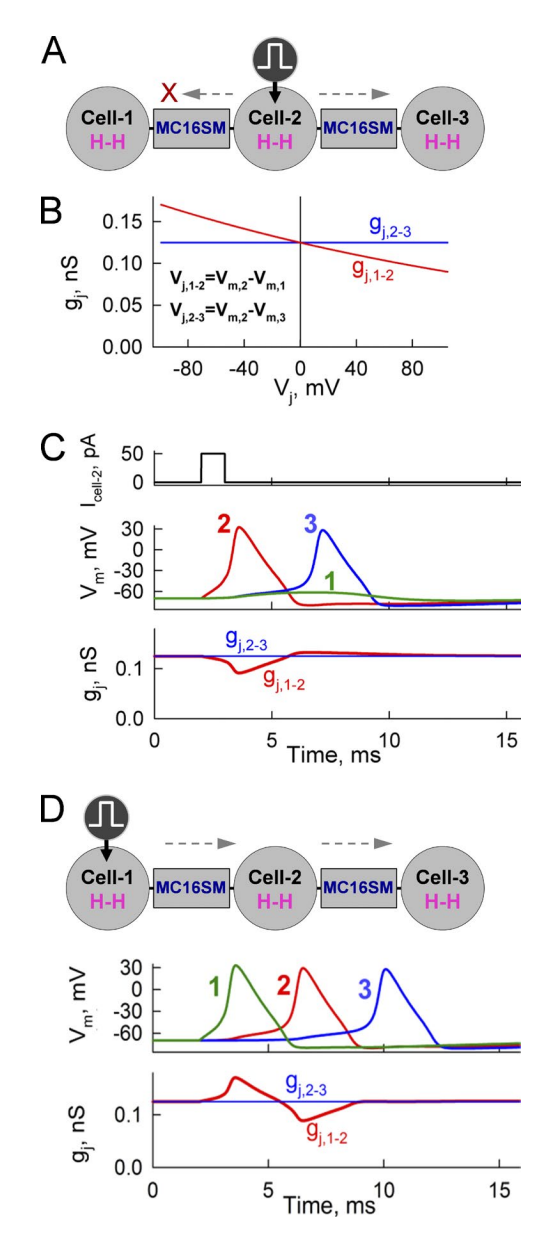


Figure 6. Unidirectional signal transfer in a cluster of three cells through electrical synapses exhibiting I-V rectification. (A) Schematic of the cells with stimulation of cell 2. (B) g_j – V_j plot exhibiting rectification of GJs between cells 1 and 2 and no rectification of GJs between cells 2 and 3. (C) Stimulation of cell 2–initiated AP that spread to cell 2, but not to cell 1, because of reduced $g_{j,1:2}$. (D) Stimulation of cell 1–initiated AP that increased $g_{j,1:2}$ because of I-V rectification, therefore facilitating AP transfer to cells 2 and 3.

electrotonic depolarizations (Fig. 7 C, c), which is typically observed at the core of spiral waves (Davidenko et al., 1992). Reverberation was stopped by a second pulse of 10 pA (Fig. 7 C, a), causing a depolarization of \sim 3 mV (Fig. 7 C, e, red arrow) and preventing reexcitation of cell 1. To examine how termination of reverberation depends on the amplitude and timing of $I_{\rm ext}$, we applied the second pulse at different phases in the reverberation cycle. Gray circles and curves show time windows (Fig. 7 C, f) during which reverberation was stopped using positive or negative $I_{\rm ext}$ pulses. Thus, termination of reverberation requires relatively low levels of excitatory or inhibitory currents locked to a specific phase of

reverberation cycle. Once initiated, reverberation does not need inhomogeneity of I-V rectification to continue.

Reverberation of excitation in a 15×15 cluster is shown in Fig. 8 (see Fig. S3 and Video 1). A single stimulus applied to cell 1/1 (Fig. 8 A, red circle) caused reverberation of excitation, with its core (Fig. 8 A, dashed circle) identical to that in Fig. 7. During this simulation, it was assumed that all junctions exhibited identical g_p but only two junctions shown by light-blue segments exhibited an asymmetry of I-V rectification equal to that shown in Fig. 6 B. Colored isopotential areas (see calibration bar for transmembrane potential) show the spread of excitation (dashed arrows) across the cluster. A stimulus

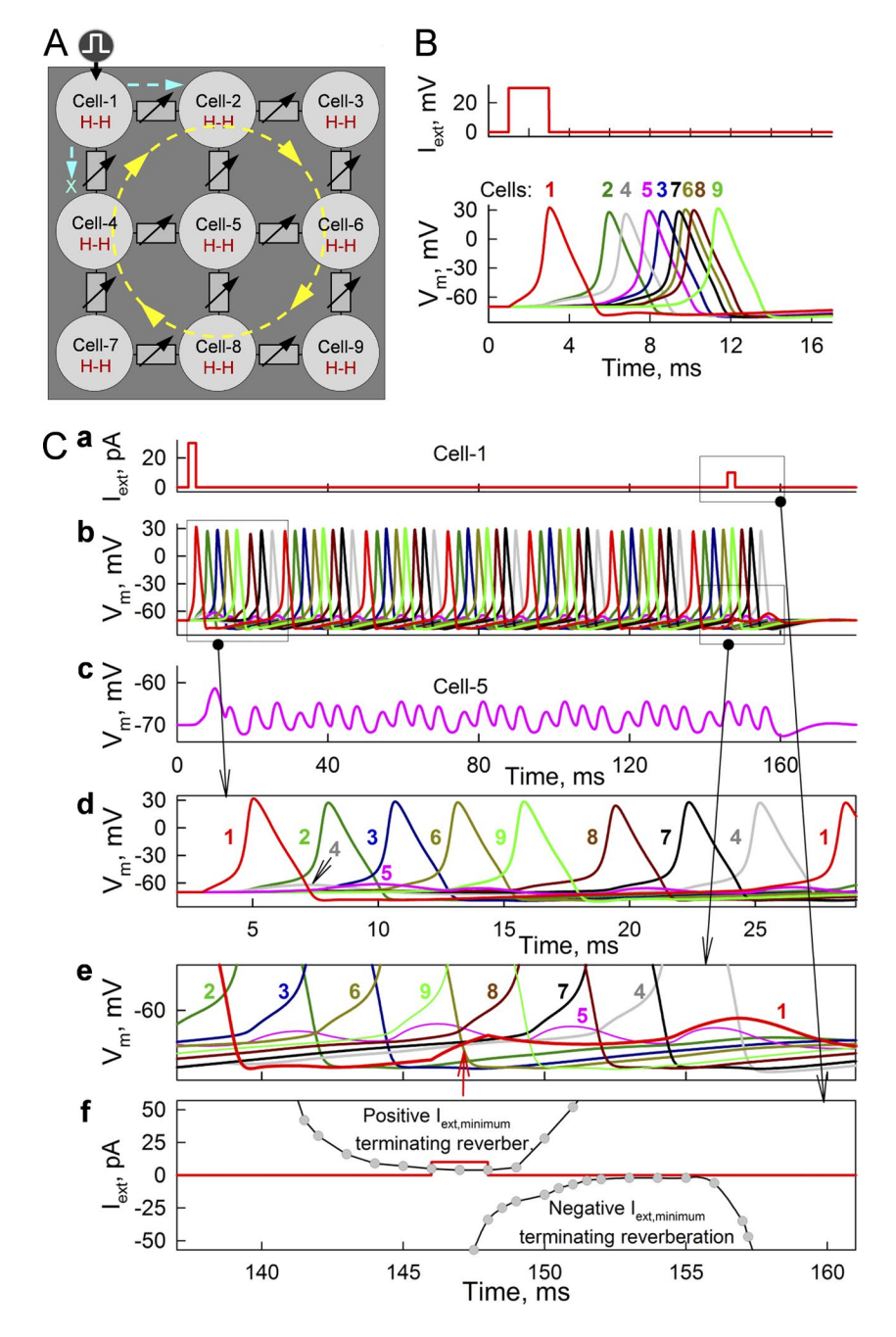


Figure 7. Formation of reverberation of excitation in a cluster of nine neurons connected through GJs modulatable by an MC16SM. (B) Spread of APs from stimulated cell 1 through all cells shown in A. gi values of GIs varied randomly from 0.175 to 0.2 nS and did not exhibit I-V rectification. (C) Initiation and termination of reverberation of excitation (b) by a single stimulus applied to cell 1 at 2 and 146 ms, respectively (a). Cell 5 is located at the core of reverberation and exhibits only electrotonic depolarizations not transforming into APs (c). The first stimulus caused AP, which spreads to cell 2 but not to cell 4 (d). Reverberation of excitation was stopped by the second pulse, which caused depolarization of \sim 3 mV in the middle of cell 1 cycle (red arrow in e) and prevented reexcitation of cell 1 by cell 4. (f) Summarized data demonstrating time windows during which positive and negative I_{ext.cell 1} pulses of minimal amplitude were able to terminate reverberation of excitation.

applied to cell 8/8 (Fig. 8 B, red circle) caused formation of two endless reverberation circles spreading across the cluster. In this experiment, it was assumed that junctions indicated by light-blue segments exhibited I-V rectification (see Fig. S4 and Video 2). Cells located in the center of the reverberation core (Fig. 8, A [cell 2/2] and B [cells 9/9 and 7/9]) exhibited low-amplitude electrotonic responses similar to those shown in Fig. 7 C (c), whereas all other cells in the cluster generated ordinary APs. To examine whether the spread of excitation in a 15×15 cluster is affected by boundary conditions, we wrapped the cluster on a virtual torus by connecting all cells in column 1 with cells in column 15 and all cells in row 1 with cells in row 15. Reverberation was initiated by a single stimulus applied to cell 4/8 (red circle); I-Vrectifying junctions are indicated by light-blue segments. Fig. S5 and Video 3 show a returning excitation wave that spreads from right to left and collides with the wave spreading from the reverberation core. These data show that for clusters of \sim 15 × 15 and larger, the boundary conditions do not noticeably affect the spread of excitation and formation of reverberation. Our data also show that reverberation can be initiated independently whether the region of I-V rectification is located in the corner of the cluster or more centrally. However, as shown in Fig. S6 and Video 4, the presence of multiple I-V rectification inhomogeneities can cause local deformations of spreading spiral waves when passing these regions. Larger regions of I-V inhomogeneity might break down the front of excitation, leading to formation of a new reverberator (not shown), as was demonstrated in computational model of cardiac arrhythmias (Casaleggio et al., 2014).

DISCUSSION

In all reported models describing synchronization or phase-locked activity of neuronal networks, as well as the spread of excitation in various excitable structures, GJC is defined as constant. However, it is well established that fast and slow gates of GJ channels are modulated by voltage, chemical uncouplers, and coupling-promoting reagents. These changes occur in a timescale from hundreds of milliseconds to minutes. Furthermore, GI channels exhibit I-V rectification, which changes the single-channel conductance instantaneously. Hence, the regulation of GJ channels is highly complex, and an influence of V_i gating as well as I-V rectification should be accounted for, especially during high spiking activity of neuronal networks. We acknowledge that 2-D models present a simplified architecture of neuronal networks; however, it was reported that a 2-D lattice describing a network of basket cells is physiologically adequate (Alcami and Marty, 2013). The 2-D lattice is also extensively used to model the tissues of cardiomyocytes (Pertsov et al., 1993; Casaleggio et al., 2014) or in numerical modeling of epileptic seizures (Volman et al., 2011).

In neuronal networks, V_j can change dynamically because of a phase shift between APs in neighboring cells, which we name $V_{j,AP}$. One of our major goals was to find whether $V_{j,AP}$ s that last only a few milliseconds can influence GJC through V_j gating and how such influence depends on the Cx isoform. The spikes of $V_{j,AP}$ s, despite their brevity, are high in amplitude (>100 mV) and potentially influence open probability of fast and/or slow gates because of V_j gating and single-channel conductance caused by I-V rectification. Indeed, data shown in Fig. 4 D demonstrate that for Cx45, a single $V_{j,AP}$ can cause \sim 2% decay in g_j . During bursting activity of neurons, small g_j decays accumulate, leading to significant decays of g_j , as is shown in Fig. 4 D.

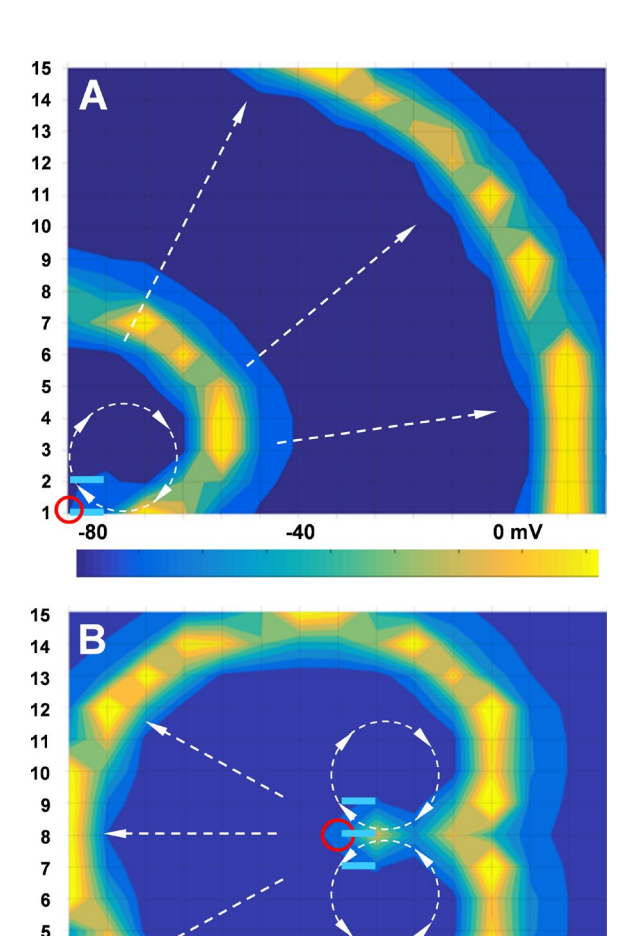


Figure 8. Reverberations of excitation in a 15×15 cluster of neurons caused by a single stimulus. In A and B, stimulus was applied to cell 1/1 and cell 8/8 (red circles), respectively. I-V–rectifying junctions are shown by light blue segments. Colored bar is calibrated for transmembrane potential.

7

3

8 9 10 11 12 13

Although mammalian electrical synapses are preferentially composed of Cx36 GJs with low sensitivity to V_i under normal conditions, their sensitivity to V_i can increase significantly at enhanced [Mg²⁺]_i (Palacios-Prado and Bukauskas, 2012; Palacios-Prado et al., 2014). This suggests that synchronization of neuronal networks may be reduced under ischemic/stroke conditions when an ATP deficit leads to an increase in [Mg²⁺]_i. An even stronger rise in sensitivity to V_i is demonstrated for Cx45 and Cx57 during acidification (Palacios-Prado and Bukauskas, 2009; Palacios-Prado et al., 2010). Because Cx45 is mostly expressed in the inferior olive (Van Der Giessen et al., 2006), whose role in coordination and control of movement is well established, our data predict that g_i in this structure should be affected by activity of neurons more than in most other structures that preferentially express Cx36. Because Cx36 is resistant to spike-induced depression (Fig. 4 E) and acidification (González-Nieto et al., 2008), synchronization of neuronal networks during paroxysmal activity or ischemia can be maintained. This may explain why Cx36 predominates over Cx45 and other Cxs in neurons of mammalian brains.

Electrical synapses are expressed in a majority of mammalian brain regions. Along with chemical synapses, they facilitate synchronous or phase-locked activity of neuronal networks. Direct GJC between neurons in hippocampus, neocortex, amygdala-hippocampuscortical axis, and other areas of the mammalian brain is well established, and knowledge on the regions expressing Cx36 has expanded extensively over the last decade because of application of better antibodies and imaging technologies with enhanced resolution (Bennett and Zukin, 2004; Connors and Long, 2004; Hormuzdi et al., 2004; Saraga et al., 2006; Bissiere et al., 2011). Electrical synapses, by forming dendro-dendritic junctions, participate in synchronizing activity of neuronal networks (Hestrin and Galarreta, 2005) spatially separated by several hundred micrometers (Fukuda and Kosaka, 2000; Saraga et al., 2006). In the somatosensory cortex, synchrony is found among inhibitory interneurons at separations of up to 400 µm (Fukuda, 2007), whereas in the primary visual cortex, this distance was from 500 to 800 µm. In the prefrontal cortex, synchronized firing during working-memory tasks appeared to be within 500 μm (Bissiere et al., 2011).

Synchronization of electrically coupled oscillators was examined theoretically in multicellular networks, and it was shown that relatively low g_j can be sufficient to synchronize or phase-lock oscillatory activity of neurons exhibiting different oscillatory activities (Saraga et al., 2006). In different regions of the brain, electrical cell-cell coupling between neurons connected through dendro-dendritic GJs is relatively weak and constitutes \sim 0.13–1.0 nS (Devor and Yarom, 2002; Venance et al., 2004; Vervaeke et al., 2010). Such GJC satisfies the conditions necessary for AP transfer between neurons, but

it is only a few fold higher than $g_{j,min-trans/s}$ which is in the range of \sim 0.1–0.3 nS and varies depending on the firing rate of pacemaker cells (Fig. 5 C). However, such GJC is >10-fold stronger than the g_j necessary for synchronization neurons if their intrinsic oscillatory activity is contiguous (Fig. 5 B).

It is evident that electrical synapses with a conductance of >10 nS would bypass function of chemical synapses and compromise information processing in neuronal networks. Presumably, this is one of reasons that electrical synapses are formed preferentially of Cx36, which exhibits the smallest single-channel conductance among all members of the Cx family (Moreno et al., 2005); <1% of Cx36 GJ channels clustered in junctional plaques are functional under normal conditions (Curti et al., 2012; Marandykina et al., 2013). An increase in open probability of Cx36 GJs during intracellular hypomagnesemia (Palacios-Prado and Bukauskas, 2012; Palacios-Prado et al., 2014), inhibition of arachidonic acid synthesis, or weak acidification (González-Nieto et al., 2008) can strengthen electrical synapses, thus resulting in hypersynchronization, which is linked to development epileptic seizures (Carlen et al., 2000; Gajda et al., 2003).

Data shown in Fig. 6 demonstrate that relatively weak rectification of GJ channels can change g_i instantaneously during short-lasting $V_{i,AP}$ that can lead to unidirectional signal transfer and consequently to reverberation of excitation (Figs. 7 and 8). Thus, I-V rectification can very quickly reshape the functional state of a neuronal network in response to dynamic changes of bursting activity and initiate self-sustained reverberation. Furthermore, it was proposed that I-V rectification of GIs is defined by an asymmetry of fixed charges, assumed to be charged amino acids, inside the channel pore, and described using the Poisson-Nernst-Plank equation (Oh et al., 1999). Recently, we demonstrated a Mg²⁺dependent plasticity of electrical synapses between neurons in the mesencephalic trigeminal nucleus (Palacios-Prado et al., 2013) and in the thalamic reticular nucleus (Palacios-Prado et al., 2013, 2014). Also, we showed a novel form of I-V rectification in Cx36 that depends on Mg²⁺ binding within the pore (Palacios-Prado et al., 2013, 2014). It was assumed that a domain of extracellular loop 1, containing D47 residue, forms a Mg²⁺-binding/interaction site, which at higher $[Mg^{2+}]_i$ (~ 5 mM) creates an exponential I-V rectification, which is oriented in the opposite direction than I-V rectification caused by fixed charges. Superposition of these two forms of I-V rectification results in a hyperbolic $I_{i,inst}V_i$ relationship measured uniquely in Cx36 GJ channels (Palacios-Prado et al., 2014). In addition, it was shown that at low $[Mg^{2+}]_i$ ($\sim 10 \mu M$) in both cells, the $I_{j,inst}V_j$ relationship becomes linear, whereas transjunctional asymmetry in $[Mg^{2+}]_i$ can cause an exponential $I_{i,inst}V_i$ relationship. This is caused by a presence of I-V rectification in the hemichannel exposed to 5 mM [Mg²⁺]_i and absence of I-V rectification in the hemichannel exposed to $0.01~\text{mM}~[\text{Mg}^{2+}]_i$. The I-V rectification in electrical synapses has been proposed to affect the dynamic output of neuronal networks, and therefore this novel Mg^{2+} -dependent I-V rectification could explain the switching between firing states and changes in the output of neuronal networks during different metabolic states when $[\text{Mg}^{2+}]_i$ is strongly affected (Gutierrez and Marder, 2013).

We demonstrate that reverberation of excitation in a multicellular network of neurons interconnected only through electrical synapses and inhomogeneities of I-V rectification can be initiated and terminated by a single excitation of only one cell. Previously, Lorente de Nó (1933) proposed the concept of the continuous reverberation of excitations in the circuit formed from several neurons to explain the vestibulo-ocular reflex. This allows for the generation of a burst of APs in response to a single excitation and was viewed as a mechanism for the active maintenance of working memory. However, this hypothesis is not listed in the latest views on the mechanisms of short- and long-term memories preferentially related to molecular, structural, and functional changes of chemical synapses (Kandel et al., 2014; Bailey et al., 2015). Later, Lorente de Nó's idea was extended in theoretical studies demonstrating a possibility for reverberation of excitation in neuronal networks interconnected with chemical synapses (Tegnér et al., 2002; Constantinidis and Wang, 2004; Wang et al., 2004, 2011). However, there are no studies demonstrating, either experimentally or theoretically, an involvement of electrical synapses in the realization of reverberation in mammalian brain. On the other hand, reverberation of excitation was demonstrated in crayfish between segmented giant axons connected exclusively through electrical synapses (Watanabe and Grundfest, 1961). The role of reverberation of excitation in memory mechanisms was expanded by the proposal (Hebb, 1950) that memory consolidation in neuronal networks includes two basic mechanisms, post-acquisition reverberation of excitation and structural synaptic plasticity (Ribeiro and Nicolelis, 2004). It was proposed that reverberations in neuronal circuits consistently increased during "slow-wave" sleep phase, which was related to consolidation of short-term memory into long-term memory. Reverberation decreased during wakefulness, which suggests that sensory input might suppress reverberations. All studies relating the role of reverberation in short-term memory and its consolidation into longterm memory are based on circuits in which neurons are connected through chemical synapses (Tegnér et al., 2002; Constantinidis and Wang, 2004; Ribeiro and Nicolelis, 2004; Wang et al., 2004, 2011). Our data show that reverberation of excitation can also form in circuits interconnected through electrical instead of chemical synapses and plays a specific role in a complex mechanisms of memory. In such networks, reverberation can also be terminated by low-amplitude phase locked external stimulation (Fig. 7 C, f), resembling activation of sensory signals during a waking period. We expect that reverberation can also exist in circuits consolidating electrical and chemical synapses, in which the presence of even a single chemical synapse in a chain of neurons connected through electrical synapses can trigger unidirectional signal transfer and consequently reverberation of excitation.

Data presented in Fig. 7 show that the center of reverberation core cells did not exhibit APs but instead displayed multiple low-amplitude depolarizations that appeared to be electrotonic responses from APs in neighboring cells. Such behavior is characteristic only for reverberation and cannot be observed during the high frequency caused by enhanced automaticity. Also, low-amplitude depolarizations are a hallmark of spiral wave dynamics (Davidenko et al., 1992), which have been associated with cardiac arrhythmias (Pertsov et al., 1993). It has been detected that epileptic seizures may also manifest as recurrent spiral waves in cat neocortex (Stacey, 2012). Interestingly, a termination of reverberation requires relatively low levels of excitatory or inhibitory current, whereas active windows are locked to specific phases of the reverberation cycle (Fig. 7 C, f). Again, such a property applies only to reverberation of excitation and not to enhanced automaticity, which cannot be terminated by phase-locked stimulation. Both these criteria can serve to differentiate reverberation from enhanced automaticity in the experiment.

The role of GJs in the structural synaptic plasticity is less known; however, several studies suggest a link between GJ activity and memory consolidation via the process of phosphorylation. Cx phosphorylation can influence GJC in cell cultures (Márquez-Rosado et al., 2012) and hippocampus (Nakai et al., 2014). Indeed, phosphorylation/dephosphorylation could combine both necessary conditions of Hebb's hypothesis, synaptic plasticity and reverberation of excitation, into a single theoretical mechanism: changes caused by Cx phosphorylation/dephosphorylation can increase I-V rectification, which allows unidirectional signal transfer between cells and, consequentially, enables reverberation of excitation.

We thank Michael V.L. Bennett and Vytautas Verselis for helpful comments and discussions. We thank Angele Bukauskiene, Kevin Fisher, Alis Dicpinigaitis, and Deesha Shah for excellent technical assistance.

This study was funded by a grant (MIP-76/2015) from the Research Council of Lithuania and by National Institutes of Health grant R01NS 072238 to F.F. Bukauskas.

The authors declare no competing financial interests.

Richard W. Aldrich served as editor.

Submitted: 30 July 2015 Accepted: 5 January 2016

REFERENCES

- Alcami, P., and A. Marty. 2013. Estimating functional connectivity in an electrically coupled interneuron network. *Proc. Natl. Acad. Sci. USA*. 110:E4798–E4807. http://dx.doi.org/10.1073/pnas.1310983110
- Alev, C., S. Urschel, S. Sonntag, G. Zoidl, A.G. Fort, T. Höher, M. Matsubara, K. Willecke, D.C. Spray, and R. Dermietzel. 2008. The neuronal connexin36 interacts with and is phosphorylated by CaMKII in a way similar to CaMKII interaction with glutamate receptors. *Proc. Natl. Acad. Sci. USA*. 105:20964–20969. http://dx.doi.org/10.1073/pnas.0805408105
- Auerbach, A.A., and M.V.L. Bennett. 1969. A rectifying electrotonic synapse in the central nervous system of a vertebrate. J. Gen. Physiol. 53:211–237. http://dx.doi.org/10.1085/jgp.53.2.211
- Bailey, C.H., E.R. Kandel, and K.M. Harris. 2015. Structural components of synaptic plasticity and memory consolidation. *Cold Spring Harb. Perspect. Biol.* 7:a021758. http://dx.doi.org/10.1101/cshperspect.a021758
- Bennett, M.V., and R.S. Zukin. 2004. Electrical coupling and neuronal synchronization in the mammalian brain. *Neuron.* 41:495–511. http://dx.doi.org/10.1016/S0896-6273(04)00043-1
- Bissiere, S., M. Zelikowsky, R. Ponnusamy, N.S. Jacobs, H.T. Blair, and M.S. Fanselow. 2011. Electrical synapses control hippocampal contributions to fear learning and memory. *Science*. 331:87–91. http://dx.doi.org/10.1126/science.1193785
- Brunel, N., and V. Hakim. 1999. Fast global oscillations in networks of integrate-and-fire neurons with low firing rates. *Neural Comput.* 11:1621–1671. http://dx.doi.org/10.1162/089976699300016179
- Bukauskas, F.F., and C. Peracchia. 1997. Two distinct gating mechanisms in gap junction channels: CO2-sensitive and voltage-sensitive. *Biophys. J.* 72:2137–2142. http://dx.doi.org/10.1016/S0006-3495(97)78856-8
- Bukauskas, F.F., and V.K. Verselis. 2004. Gap junction channel gating. *Biochim. Biophys. Acta.* 1662:42–60. http://dx.doi.org/10.1016/j.bbamem.2004.01.008
- Bukauskas, F.F., and R. Weingart. 1993. Multiple conductance states of newly formed single gap junction channels between insect cells. *Pflugers Arch.* 423:152–154. http://dx.doi.org/10.1007/BF00374973
- Bukauskas, F.F., and R. Weingart. 1994. Voltage-dependent gating of single gap junction channels in an insect cell line. *Biophys. J.* 67:613–625. http://dx.doi.org/10.1016/S0006-3495(94)80521-1
- Bukauskas, F.F., C. Elfgang, K. Willecke, and R. Weingart. 1995. Biophysical properties of gap junction channels formed by mouse connexin40 in induced pairs of transfected human HeLa cells. *Biophys. J.* 68:2289–2298. http://dx.doi.org/10.1016/S0006-3495(95)80411-X
- Bukauskas, F.F., A. Bukauskiene, and V.K. Verselis. 2002a. Conductance and permeability of the residual state of connexin43 gap junction channels. *J. Gen. Physiol.* 119:171–185. http://dx.doi.org/10.1085/jgp.119.2.171
- Bukauskas, F.F., A.B. Angele, V.K. Verselis, and M.V.L. Bennett. 2002b. Coupling asymmetry of heterotypic connexin 45/ connexin 43-EGFP gap junctions: Properties of fast and slow gating mechanisms. *Proc. Natl. Acad. Sci. USA*. 99:7113–7118. http://dx.doi.org/10.1073/pnas.032062099
- Cachope, R., K. Mackie, A. Triller, J. O'Brien, and A.E. Pereda. 2007. Potentiation of electrical and chemical synaptic transmission mediated by endocannabinoids. *Neuron.* 56:1034–1047. http://dx.doi.org/10.1016/j.neuron.2007.11.014
- Carlen, P.L., F. Skinner, L. Zhang, C. Naus, M. Kushnir, and J.L. Perez Velazquez. 2000. The role of gap junctions in seizures. *Brain Res. Brain Res. Rev.* 32:235–241. http://dx.doi.org/10.1016/S0165-0173(99)00084-3
- Casaleggio, A., M.L. Hines, and M. Migliore. 2014. Computational model of erratic arrhythmias in a cardiac cell network: The role of

- gap junctions. PLoS One. 9:e100288. http://dx.doi.org/10.1371/journal.pone.0100288
- Chapman, R.J., V.K. Lall, S. Maxeiner, K. Willecke, J. Deuchars, and A.E. King. 2013. Localization of neurones expressing the gap junction protein Connexin45 within the adult spinal dorsal horn: A study using Cx45-eGFP reporter mice. *Brain Struct. Funct.* 218:751–765. http://dx.doi.org/10.1007/s00429-012-0426-1
- Chen-Izu, Y., A.P. Moreno, and R.A. Spangler. 2001. Opposing gates model for voltage gating of gap junction channels. Am. J. Physiol. Cell Physiol. 281:C1604–C1613.
- Connors, B.W., and M.A. Long. 2004. Electrical synapses in the mammalian brain. *Annu. Rev. Neurosci.* 27:393–418. http://dx.doi.org/10.1146/annurev.neuro.26.041002.131128
- Constantinidis, C., and X.J. Wang. 2004. A neural circuit basis for spatial working memory. *Neuroscientist.* 10:553–565. http://dx.doi.org/10.1177/1073858404268742
- Curti, S., G. Hoge, J.I. Nagy, and A.E. Pereda. 2012. Synergy between electrical coupling and membrane properties promotes strong synchronization of neurons of the mesencephalic trigeminal nucleus. J. Neurosci. 32:4341–4359. http://dx.doi.org/10.1523/ JNEUROSCI.6216-11.2012
- Davidenko, J.M., A.V. Pertsov, R. Salomonsz, W. Baxter, and J. Jalife. 1992. Stationary and drifting spiral waves of excitation in isolated cardiac muscle. *Nature*. 355:349–351. http://dx.doi.org/10.1038/355349a0
- Davidenko, J.M., R. Salomonsz, A.M. Pertsov, W.T. Baxter, and J. Jalife. 1995. Effects of pacing on stationary reentrant activity. Theoretical and experimental study. *Circ. Res.* 77:1166–1179. http://dx.doi.org/10.1161/01.RES.77.6.1166
- Devor, A., and Y. Yarom. 2002. Electrotonic coupling in the inferior olivary nucleus revealed by simultaneous double patch recordings. *J. Neurophysiol.* 87:3048–3058.
- DeVries, S.H., and E.A. Schwartz. 1992. Hemi-gap-junction channels in solitary horizontal cells of the catfish retina. *J. Physiol.* 445:201–230. http://dx.doi.org/10.1113/jphysiol.1992.sp018920
- Fukuda, T. 2007. Structural organization of the gap junction network in the cerebral cortex. *Neuroscientist*. 13:199–207. http://dx.doi.org/10.1177/1073858406296760
- Fukuda, T., and T. Kosaka. 2000. Gap junctions linking the dendritic network of GABAergic interneurons in the hippocampus. J. Neurosci. 20:1519–1528.
- Furshpan, E.J., and D.D. Potter. 1959. Transmission at the giant motor synapses of the crayfish. J. Physiol. 145:289–325. http:// dx.doi.org/10.1113/jphysiol.1959.sp006143
- Gajda, Z., E. Gyengési, E. Hermesz, K.S. Ali, and M. Szente. 2003. Involvement of gap junctions in the manifestation and control of the duration of seizures in rats in vivo. *Epilepsia*. 44:1596–1600. http://dx.doi.org/10.1111/j.0013-9580.2003 .25803.x
- Gibson, J.R., M. Beierlein, and B.W. Connors. 1999. Two networks of electrically coupled inhibitory neurons in neocortex. *Nature*. 402:75–79. http://dx.doi.org/10.1038/47035
- González, D., J.M. Gómez-Hernández, and L.C. Barrio. 2007. Molecular basis of voltage dependence of connexin channels: An integrative appraisal. *Prog. Biophys. Mol. Biol.* 94:66–106. http:// dx.doi.org/10.1016/j.pbiomolbio.2007.03.007
- González-Nieto, D., J.M. Gómez-Hernández, B. Larrosa, C. Gutiérrez, M.D. Muñoz, I. Fasciani, J. O'Brien, A. Zappalà, F. Cicirata, and L.C. Barrio. 2008. Regulation of neuronal connexin-36 channels by pH. *Proc. Natl. Acad. Sci. USA*. 105:17169–17174. http://dx.doi.org/10.1073/pnas.0804189105
- Gutierrez, G.J., and E. Marder. 2013. Rectifying electrical synapses can affect the influence of synaptic modulation on output pattern robustness. *J. Neurosci.* 33:13238–13248. http://dx.doi.org/10.1523/JNEUROSCI.0937-13.2013

- Haas, J.S., B. Zavala, and C.E. Landisman. 2011. Activity-dependent long-term depression of electrical synapses. *Science*. 334:389–393. http://dx.doi.org/10.1126/science.1207502
- Harris, A.L., D.C. Spray, and M.V.L. Bennett. 1981. Kinetic properties of a voltage-dependent junctional conductance. *J. Gen. Physiol.* 77:95–117. http://dx.doi.org/10.1085/jgp.77.1.95
- Hebb, D.O. 1949. The Organization of Behavior. Wiley and Sons, New York. 335 pp.
- Hestrin, S., and M. Galarreta. 2005. Electrical synapses define networks of neocortical GABAergic neurons. *Trends Neurosci.* 28:304–309. http://dx.doi.org/10.1016/j.tins.2005.04.001
- Hodgkin, A.L., and A.F. Huxley. 1952. A quantitative description of membrane current and its application to conduction and excitation in nerve. *J. Physiol.* 117:500–544. http://dx.doi.org/10.1113/jphysiol.1952.sp004764
- Hormuzdi, S.G., M.A. Filippov, G. Mitropoulou, H. Monyer, and R. Bruzzone. 2004. Electrical synapses: A dynamic signaling system that shapes the activity of neuronal networks. *Biochim. Biophys. Acta*. 1662:113–137. http://dx.doi.org/10.1016/j.bbamem.2003.10.023
- Juang, J., and Y.H. Liang. 2014. Cluster synchronization in networks of neurons with chemical synapses. *Chaos.* 24:013110. http://dx .doi.org/10.1063/1.4862484
- Kandel, E.R., Y. Dudai, and M.R. Mayford. 2014. The molecular and systems biology of memory. *Cell.* 157:163–186. http://dx.doi .org/10.1016/j.cell.2014.03.001
- Kronengold, J., E.B. Trexler, F.F. Bukauskas, T.A. Bargiello, and V.K. Verselis. 2003. Pore-lining residues identified by single channel SCAM studies in Cx46 hemichannels. *Cell Commun. Adhes.* 10:193–199. http://dx.doi.org/10.1080/cac.10.4-6.193.199
- Lorente de Nó, R. 1933. Vestibulo-ocular reflex arc. Arch NeurPsych. 30:245–291. http://dx.doi.org/10.1001/archneurpsyc.1933.02240140009001
- Marandykina, A., N. Palacios-Prado, L. Rimkutė, V.A. Skeberdis, and F.F. Bukauskas. 2013. Regulation of connexin36 gap junction channels by n-alkanols and arachidonic acid. *J. Physiol.* 591:2087–2101. http://dx.doi.org/10.1113/jphysiol.2013.250910
- Márquez-Rosado, L., J.L. Solan, C.A. Dunn, R.P. Norris, and P.D. Lampe. 2012. Connexin43 phosphorylation in brain, cardiac, endothelial and epithelial tissues. *Biochim. Biophys. Acta.* 1818:1985–1992. http://dx.doi.org/10.1016/j.bbamem.2011.07.028
- Moreno, A.P., M.B. Rook, G.I. Fishman, and D.C. Spray. 1994. Gap junction channels: Distinct voltage-sensitive and -insensitive conductance states. *Biophys. J.* 67:113–119. http://dx.doi.org/10.1016/S0006-3495(94)80460-6
- Moreno, A.P., V.M. Berthoud, G. Pérez-Palacios, and E.M. Pérez-Armendariz. 2005. Biophysical evidence that connexin-36 forms functional gap junction channels between pancreatic mouse beta-cells. *Am. J. Physiol. Endocrinol. Metab.* 288:E948–E956. http://dx.doi.org/10.1152/ajpendo.00216.2004
- Nakai, T., T. Nagai, M. Tanaka, N. Itoh, N. Asai, A. Enomoto, M. Asai, S. Yamada, A.B. Saifullah, M. Sokabe, et al. 2014. Girdin phosphorylation is crucial for synaptic plasticity and memory: A potential role in the interaction of BDNF/TrkB/Akt signaling with NMDA receptor. J. Neurosci. 34:14995–15008. http://dx.doi.org/10.1523/JNEUROSCI.2228-14.2014
- Oh, S., J.B. Rubin, M.V. Bennett, V.K. Verselis, and T.A. Bargiello. 1999. Molecular determinants of electrical rectification of single channel conductance in gap junctions formed by connexins 26 and 32. *J. Gen. Physiol.* 114:339–364. http://dx.doi.org/10.1085/jgp.114.3.339
- Ouyang, X., V.M. Winbow, L.S. Patel, G.S. Burr, C.K. Mitchell, and J. O'Brien. 2005. Protein kinase A mediates regulation of gap junctions containing connexin35 through a complex pathway. *Brain Res. Mol. Brain Res.* 135:1–11. http://dx.doi.org/10.1016/j .molbrainres.2004.10.045

- Palacios-Prado, N., and F.F. Bukauskas. 2009. Heterotypic gap junction channels as voltage-sensitive valves for intercellular signaling. Proc. Natl. Acad. Sci. USA. 106:14855–14860. http://dx.doi.org/10.1073/pnas.0901923106
- Palacios-Prado, N., and F.F. Bukauskas. 2012. Modulation of metabolic communication through gap junction channels by transjunctional voltage; synergistic and antagonistic effects of gating and ionophoresis. *Biochim. Biophys. Acta.* 1818:1884–1894. http://dx.doi.org/10.1016/j.bbamem.2011.09.001
- Palacios-Prado, N., S. Sonntag, V.A. Skeberdis, K. Willecke, and F.F. Bukauskas. 2009. Gating, permselectivity and pH-dependent modulation of channels formed by connexin57, a major connexin of horizontal cells in the mouse retina. *J. Physiol.* 587:3251– 3269. http://dx.doi.org/10.1113/jphysiol.2009.171496
- Palacios-Prado, N., S.W. Briggs, V.A. Skeberdis, M. Pranevicius, M.V. Bennett, and F.F. Bukauskas. 2010. pH-dependent modulation of voltage gating in connexin45 homotypic and connexin45/connexin43 heterotypic gap junctions. *Proc. Natl. Acad. Sci. USA*. 107:9897–9902. http://dx.doi.org/10.1073/pnas.1004552107
- Palacios-Prado, N., G. Hoge, A. Marandykina, L. Rimkute, S. Chapuis, N. Paulauskas, V.A. Skeberdis, J. O'Brien, A.E. Pereda, M.V.L. Bennett, and F.F. Bukauskas. 2013. Intracellular magnesium-dependent modulation of gap junction channels formed by neuronal connexin36. *J. Neurosci.* 33:4741–4753. http://dx.doi.org/10.1523/JNEUROSCI.2825-12.2013
- Palacios-Prado, N., S. Chapuis, A. Panjkovich, J. Fregeac, J.I. Nagy, and F.F. Bukauskas. 2014. Molecular determinants of magnesium-dependent synaptic plasticity at electrical synapses formed by connexin36. *Nat. Commun.* 5:4667. http://dx.doi.org/10.1038/ncomms5667
- Paulauskas, N., M. Pranevicius, H. Pranevicius, and F.F. Bukauskas. 2009. A stochastic four-state model of contingent gating of gap junction channels containing two "fast" gates sensitive to transjunctional voltage. *Biophys. J.* 96:3936–3948. http://dx.doi.org/ 10.1016/j.bpj.2009.01.059
- Paulauskas, N., H. Pranevicius, J. Mockus, and F.F. Bukauskas. 2012. Stochastic 16-state model of voltage gating of gap-junction channels enclosing fast and slow gates. *Biophys. J.* 102:2471–2480. http://dx.doi.org/10.1016/j.bpj.2012.04.038
- Pertsov, A.M., J.M. Davidenko, R. Salomonsz, W.T. Baxter, and J. Jalife. 1993. Spiral waves of excitation underlie reentrant activity in isolated cardiac muscle. *Circ. Res.* 72:631–650. http://dx.doi.org/10.1161/01.RES.72.3.631
- Phelan, P., L.A. Goulding, J.L. Tam, M.J. Allen, R.J. Dawber, J.A. Davies, and J.P. Bacon. 2008. Molecular mechanism of rectification at identified electrical synapses in the *Drosophila* giant fiber system. *Curr. Biol.* 18:1955–1960. http://dx.doi.org/10.1016/j.cub.2008.10.067
- Rackauskas, M., M.M. Kreuzberg, M. Pranevicius, K. Willecke, V.K. Verselis, and F.F. Bukauskas. 2007. Gating properties of heterotypic gap junction channels formed of connexins 40, 43, and 45. *Biophys. J.* 92:1952–1965. http://dx.doi.org/10.1529/ biophysj.106.099358
- Ramanan, S.V., P.R. Brink, K. Varadaraj, E. Peterson, K. Schirrmacher, and K. Banach. 1999. A three-state model for connexin37 gating kinetics. *Biophys. J.* 76:2520–2529. http://dx.doi.org/10.1016/S0006-3495(99)77406-0
- Rash, J.E., S. Curti, K.G. Vanderpool, N. Kamasawa, S. Nannapaneni, N. Palacios-Prado, C.E. Flores, T. Yasumura, J. O'Brien, B.D. Lynn, et al. 2013. Molecular and functional asymmetry at a vertebrate electrical synapse. *Neuron.* 79:957–969. http://dx.doi.org/10.1016/ j.neuron.2013.06.037
- Ribeiro, S., and M.A. Nicolelis. 2004. Reverberation, storage, and postsynaptic propagation of memories during sleep. *Learn. Mem.* 11:686–696. http://dx.doi.org/10.1101/lm.75604

- Sakalauskaite, A., H. Pranevicius, M. Pranevicius, and F. Bukauskas. 2011. Markovian model of the voltage gating of connexin-based gap junction channels. *Electron. Electr. Eng.* 111:103–106.
- Saraga, F., L. Ng, and F.K. Skinner. 2006. Distal gap junctions and active dendrites can tune network dynamics. *J. Neurophysiol.* 95:1669–1682. http://dx.doi.org/10.1152/jn.00662.2005
- Skeberdis, V.A., L. Rimkute, A. Skeberdyte, N. Paulauskas, and F.F. Bukauskas. 2011. pH-dependent modulation of connexin-based gap junctional uncouplers. J. Physiol. 589:3495–3506. http://dx.doi.org/10.1113/jphysiol.2011.209072
- Snipas, M., H. Pranevicius, M. Pranevicius, O. Pranevicius, N. Paulauskas, and F.F. Bukauskas. 2015. Application of stochastic automata networks for creation of continuous time Markov chain models of voltage gating of gap junction channels. *BioMed Res. Int.* 2015:936295. http://dx.doi.org/10.1155/2015/936295
- Söhl, G., S. Maxeiner, and K. Willecke. 2005. Expression and functions of neuronal gap junctions. *Nat. Rev. Neurosci.* 6:191–200. http://dx.doi.org/10.1038/nrn1627
- Stacey, W. 2012. Better resolution and fewer wires discover epileptic spiral waves. *Epilepsy Curr.* 12:147–149. http://dx.doi.org/10.5698/1535-7511-12.4.147
- Tegnér, J., A. Compte, and X.J. Wang. 2002. The dynamical stability of reverberatory neural circuits. *Biol. Cybern.* 87:471–481. http://dx.doi.org/10.1007/s00422-002-0363-9
- Tong, J.J., and L. Ebihara. 2006. Structural determinants for the differences in voltage gating of chicken Cx56 and Cx45.6 gap-junctional hemichannels. *Biophys. J.* 91:2142–2154. http://dx.doi.org/10.1529/biophysj.106.082859
- Trexler, E.B., M.V. Bennett, T.A. Bargiello, and V.K. Verselis. 1996. Voltage gating and permeation in a gap junction hemichannel. *Proc. Natl. Acad. Sci. USA*. 93:5836–5841. http://dx.doi.org/10.1073/pnas.93.12.5836
- Valiunas, V., R. Mui, E. McLachlan, G. Valdimarsson, P.R. Brink, and T.W. White. 2004. Biophysical characterization of zebrafish connexin35 hemichannels. Am. J. Physiol. Cell Physiol. 287: C1596–C1604. http://dx.doi.org/10.1152/ajpcell.00225.2004
- Van Der Giessen, R.S., S. Maxeiner, P.J. French, K. Willecke, and C.I. De Zeeuw. 2006. Spatiotemporal distribution of Connexin45 in

- the olivocerebellar system. *J. Comp. Neurol.* 495:173–184. http://dx.doi.org/10.1002/cne.20873
- Veenstra, R.D., H.Z. Wang, E.C. Beyer, S.V. Ramanan, and P.R. Brink. 1994. Connexin37 forms high conductance gap junction channels with subconductance state activity and selective dye and ionic permeabilities. *Biophys. J.* 66:1915–1928. http://dx.doi.org/10.1016/S0006-3495(94)80985-3
- Venance, L., J. Glowinski, and C. Giaume. 2004. Electrical and chemical transmission between striatal GABAergic output neurones in rat brain slices. J. Physiol. 559:215–230. http://dx.doi.org/10.1113/jphysiol.2004.065672
- Vervaeke, K., A. Lorincz, P. Gleeson, M. Farinella, Z. Nusser, and R.A. Silver. 2010. Rapid desynchronization of an electrically coupled interneuron network with sparse excitatory synaptic input. *Neuron*. 67:435–451. http://dx.doi.org/10.1016/j.neuron.2010.06.028
- Vogel, R., and R. Weingart. 1998. Mathematical model of vertebrate gap junctions derived from electrical measurements on homotypic and heterotypic channels. J. Physiol. 510:177–189. http:// dx.doi.org/10.1111/j.1469-7793.1998.177bz.x
- Volman, V., M. Perc, and M. Bazhenov. 2011. Gap junctions and epileptic seizures—two sides of the same coin? *PLoS One.* 6:e20572. http://dx.doi.org/10.1371/journal.pone.0020572
- von Maltzahn, J., C. Euwens, K. Willecke, and G. Söhl. 2004. The novel mouse connexin39 gene is expressed in developing striated muscle fibers. *J. Cell Sci.* 117:5381–5392. http://dx.doi.org/10.1242/jcs.01413
- Wang, X.J., J. Tegnér, C. Constantinidis, and P.S. Goldman-Rakic. 2004. Division of labor among distinct subtypes of inhibitory neurons in a cortical microcircuit of working memory. *Proc. Natl. Acad. Sci. USA*. 101:1368–1373. http://dx.doi.org/10.1073/ pnas.0305337101
- Wang, M., N.J. Gamo, Y. Yang, L.E. Jin, X.J. Wang, M. Laubach, J.A. Mazer, D. Lee, and A.F.T. Arnsten. 2011. Neuronal basis of agerelated working memory decline. *Nature*. 476:210–213. http://dx.doi.org/10.1038/nature10243
- Watanabe, A., and H. Grundfest. 1961. Impulse propagation at the septal and commissural junctions of crayfish lateral giant axons. *J. Gen. Physiol.* 45:267–308. http://dx.doi.org/10.1085/jgp.45.2.267

Maciunas et al., http://www.jgp.org/cgi/content/full/jgp.201511488/DC1

H-H model

We have modified the original H-H model (Hodgkin and Huxley, 1952) by adding I_p described by the following system of ordinary differential equations:

$$\begin{cases} I_{m} = I_{ext} + C_{m} \frac{dV_{m}}{dt} + g_{K} n^{4} (V_{m} - V_{K}) + g_{Na} m^{3} h(V_{m} - V_{Na}) + g_{l} (V_{m} - V_{l}) + I_{j}; \\ \frac{dn}{dt} = \alpha_{n} (V_{m}) \cdot (1 - n) - \beta_{n} (V_{m}) \cdot n; \\ \frac{dm}{dt} = \alpha_{m} (V_{m}) \cdot (1 - m) - \beta_{m} (V_{m}) \cdot m; \\ \frac{dh}{dt} = \alpha_{h} (V_{m}) \cdot (1 - h) - \beta_{h} (V_{m}) \cdot h. \end{cases}$$

Here, I_m is the transmembrane current per unit area, I_{ext} is external stimulus current, V_m is membrane potential, and C_m is the membrane capacitance per unit area; V_K , V_{Na} , and V_l are the potassium, sodium, and leak reversal potentials, respectively; g_K , g_{Na} , and g_l are the maximal respectively. mum values of potassium, sodium, and leak conductances per unit area, respectively; n, m, and h are variables $(0 \le n, m, h \le 1)$ associated with potassium channel activation, sodium channel activation, and sodium channel inactivation, respectively; and α_i and β_i are rate constants for the respective ion channels. We referred to the following websites for advice on model implementation in MATLAB as well as on the selection of model parameters: https://senselab.med.yale. edu/modeldb/ShowModel.cshtml?model=42322 and http://icwww. epfl.ch/~gerstner/SPNM/node14.html. The membrane capacity C_m was chosen as 1 μ F/cm². The corrected values of reversal potentials were chosen as $V_K = -12$, $V_{Na} = 115$, and $V_l = 10.6$ mV, whereas conductances were chosen as $g_K = 36$, $g_{Na} = 120$, and $g_l = 0.3 \text{ mS/cm}^2$ (Hodgkin and Huxley, 1952). The functions α_i and β_i were as follows:

$$\alpha_n \left(V_m \right) = \frac{0.1 - 0.01 \cdot V_m}{e^{(1 - 0.1 \cdot V_m)} - 1};$$

$$\alpha_m(V_m) = \frac{2.5 - 0.1 \cdot V_m}{e^{(2.5 - 0.1 \cdot V_m)} - 1};$$

$$\alpha_h(V_m) = 0.07 \cdot e^{\left(-\frac{V_m}{20}\right)};$$

$$\beta_n(V_m) = 0.125 \cdot e^{\left(-\frac{V_m}{80}\right)};$$

$$\beta_m(V_m) = 4 \cdot e^{\left(-\frac{V_m}{18}\right)};$$

$$\beta_h(V_m) = \frac{1}{e^{(3-0.1\cdot V_m)} + 1}.$$

We used Euler's method for the numerical solution of H-H model equations, which was implemented in MATLAB. A time step of 0.01 ms was used in most numerical experiments.

16-state models of GJ channels voltage gating

Cells were connected through GJs, whose junctional currents, voltages, and conductances were modeled by an S16SM and MC16SM of voltage gating.

An S16SM of gating

In an S16SM (Paulauskas et al., 2012), each of four gates is characterized by gating properties and the unitary conductance of the open (o) and closed (c) states (Fig. 1 C). We have used an S16SM approach to describe the operation of each gate, allowing a simulation of I_j and g_j changes over time. This model is available online at http://connexons.aecom.yu.edu/Applet.htm, and its application in analyzing gating of GJs under normal and pathologic conditions was reported in Palacios-Prado et al. (2009) and (2010) and Skeberdis et al. (2011). Properties of gates in each of two aHCs forming the GJ channel are the same in the homotypic and different in the heterotypic GJ channel. In the algorithm describing V_j gating, we assumed that gates do not interact with each other except via voltage redistribution inside the pore, and only the voltage across the gate defines its $o\leftrightarrow c$ transitions.

The probabilities of singular $o \leftrightarrow c$ transitions depend on the equilibrium constant of slow or fast gate (Chen-Izu et al., 2001; Paulauskas et al., 2009), $K_{S,o\leftrightarrow c}$ and $K_{F,o\leftrightarrow c}$ respectively, determined as:

$$K_{S,o\leftrightarrow c} = e^{A_S(-\Pi V_S - V_{S,o})}$$

and

$$K_{F,o\leftrightarrow c} = e^{A_F(-\Pi V_F - V_{F,o})}.$$

Here, A_F and A_S characterize sensitivity to voltage, V_{Fo} and $V_{S,o}$ are voltages at which $K_{S,o\leftrightarrow r}$ or $K_{S,o\leftrightarrow r}$ are equal to 1, and Π is a gating polarity (+1 or -1). V_F and V_S are voltages across fast or slow gates, respectively, that depend on their system states at given moment, i.e., $V_F = V_F(s_j)$ and $V_S = V_S(s_j)$.

We used the following equations to calculate a single transition probabilities $p_{\rho \to \rho}$ and $p_{\rho \to \rho}$:

$$p_{0 \longrightarrow \mathcal{C}}(K, P_t) = \frac{P_t \cdot K}{1 + K},$$

$$p_{\mathcal{C} \to 0}(K, P_t) = \frac{P_t}{1+k}.$$

Here P_t is a parameter allowing us to regulate speed of $o \leftrightarrow c$ transitions. Transition probabilities, $p_{o \to o}$ and $p_{c \to c}$ are given by the rule of opposite events:

$$p_{0 \longrightarrow 0}(K, P_t) = 1 - p_{0 \longrightarrow c}(K, P_t)$$

and
 $p_{c \longrightarrow c}(K, P_t) = 1 - p_{c \longrightarrow 0}(K, P_t).$

In general, the model defines at any given discrete time interval ($\Delta t = t_n - t_{n-1}$) and V_j the probability for an individual gate to remain in the same state or to change it. Transjunctional voltage across the GJ channel is a sum of voltages across all gates. Closing one gate changes voltage across the other three gates in series, which will affect their probability of changing the state over Δt .

There is a solid body of evidence demonstrating I-V rectification of open and residual states of the GJ channel and an unapposed hemichannel (DeVries and Schwartz, 1992; Trexler et al., 1996; Oh et al., 1999; Bukauskas et al., 2002a; Kronengold et al., 2003; Valiunas et al., 2004; Tong and Ebihara, 2006; Rackauskas et al., 2007). We assumed that $\gamma_{S,open}$, $\gamma_{F,open}$, and $\gamma_{F,res}$ rectify in accordance with the exponential function as proposed in Vogel and Weingart (1998): $\gamma_{F,open} = \gamma_{F,open,0} \cdot e^{V_F/R_{F,open}}$, $\gamma_{F,open} = \gamma_{F,open,0} \cdot e^{V_F/R_{F,open}}$

$$\gamma_{F,\mathrm{res}} = \gamma_{F,\mathrm{res},0} \cdot e^{V_F/R_{F,\mathrm{res}}}\,, \qquad \qquad \gamma_{F,\mathrm{res}} = \gamma_{F,\mathrm{res},0} \cdot e^{V_F/R_{F,\mathrm{res}}}\,,$$

 $\begin{array}{l} \gamma_{S,open} = \gamma_{S,open,0} \cdot e^{V_S/R_{S,open}} \,, \quad \text{and} \quad \gamma_{S,open} = \gamma_{S,open,0} \cdot e^{V_S/R_{S,open}} \,, \quad \text{where} \\ \gamma_{F,open,0} \text{ and } \gamma_{F,res,0} \text{ are } \gamma_{F,open} \text{ at } V_F = 0, \text{ whereas } \gamma_{S,open,0} \text{ is } \gamma_{F,open} \text{ at } V_S = 0, \end{array}$ 0. $R_{F,open}$, $R_{F,res}$, and $R_{S,open}$ are rectification coefficients of the open/ residual states and fast/slow gates, respectively.

Rectification of $\gamma_{F,open}$, $\gamma_{F,res}$, and $\gamma_{S,open}$ does not allow for the evaluation of V_F and V_S in one step and necessitates the use of an iterative procedure to estimate the conductance of the GJ channel. In brief, initially we know the states of each gate, which allows for the estimation of V_F and V_S without accounting for rectification:

$$V_{F,A} = \frac{V_j \cdot \gamma_j}{\gamma_{F,A}},$$

$$V_{S,A} = \frac{V_j \cdot \gamma_j}{\gamma_{S,A}},$$

$$V_{S,B} = \frac{V_j \cdot \gamma_j}{\gamma_{S,B}},$$

and

$$V_{F,B} = \frac{V_j \cdot \gamma_j}{\gamma_{F,B}}.$$

Then, we recalculate conductances of gates accounting for rectification and reevaluate a new set of V_F and V_S . We repeat the last cycle and at the nth iterative step evaluate conductance of the GJ channel $(\gamma_{j,n})$ as well as the difference, $\Delta \gamma_{j,n} = \gamma_{j,n} - \gamma_{j,n-1}$ for convergence testing. The value of $\gamma_{i,n}$ is given by

$$\gamma_{j,n} = \frac{1}{\left(\frac{1}{\gamma_{\text{FA}}} + \frac{1}{\gamma_{\text{SA}}} + \frac{1}{\gamma_{\text{SB}}} + \frac{1}{\gamma_{\text{FB}}}\right)}.$$

The iterative procedure is stopped once the tolerance criterion $\Delta \gamma_{i,n} < (\gamma_{i,n-1}/1000)$ is reached. The final values of V_F and V_S allow for the evaluation of possible changes in the state of each gate, as well as estimation of voltages across all four gates, the sum of which should be equal to V_i , i.e., $V_i = V_{EA} + V_{S,A} + V_{EB} + V_{S,B}$.

This information is transferred to the next discrete time interval and the process is repeated. In >99% of calculations, the number of iterations was four to seven. Once the effect of I-V rectification on the unitary conductance of each GJ channel $\gamma_{i,i}$ of the electrical synapse composed of m channels is evaluated, then g_i is estimated from

$$g_j = \sum_{i=1}^m \gamma_{j,i}$$
.

In general, the S16SM simulates stochastic behavior of the electrical synapse composed of selected number GJ channels. The S16SM evaluates g_i dependence on V_i and a state of each GJ channel at a discrete time moment t_{n-1} (s^{n-1}), which is defined by states of four individual gates. An S16SM simulates the transition of gates and returns the state of GJ channels (sⁿ) at the next time moment, t_n . We used the following pseudocode for an implementation of S16SM:

$$\mathrm{S16SM}(\mathit{V}_{j},\, \boldsymbol{s}^{tn-1})$$

begin

- 1) for each channel do
- 1.1) estimate initial conductance and voltage across each gate;
- 1.2) calculate K for each gate depending on voltages across them;

- 1.3) evaluate transition probabilities based on estimated K
- 1.4) simulate gate's transition and generate a state of the GJ channel at the next discrete time moment;
- 1.5) **repeat while** the values converge
- 1.5.1) evaluate rectification of conductances for each gate;
- 1.6) estimate channel conductance at a new state;

end

2) estimate g_i

end

return g_i and s^n .

To simulate transitions of gates of a single GJ channel, we used an algorithm, whose pseudo-code is presented later.

```
Simulate GJ channel transitions (p_{c\rightarrow o}, p_{c\rightarrow o}, s^{tn-1})
begin
1. for each gate in a channel
1.1) generate basic random number r (0 < r < 1);
1.2) if gate is open
1.2.1) if p_{o\rightarrow c} < r close the gate;
1.2.2) else leave the gate open;
1.3) if gate is closed
1.3.1) if p_{c\rightarrow o} < r open the gate;
1.3.2) else leave the gate closed;
end for
return stn
end.
```

switch S

```
The MATLAB code of $16SM:
function [gj, S, g] = S16SM(vj, N, par,S,g)
A = par(:,1);
v0 = par(:,2);
go = par(:,3);
gc = par(:,4);
ro = par(:,5);
rc = par(:,6);
Pt = par(:,7);
P = par(:,8);
gg = zeros(N,1);
%for t = 1:T %time (vj iter)
for i = 1:N %channels
gg(i) \ = \ 1/(1/g(1,i) + 1/g(2,i) + 1/g(3,i) + 1/g(4,i) + 1/Gn); \ \%volt-
age on channel
v = P.*vi.*gg(i)./g(:,i);%voltages on gates
k = \exp(A.*(v-v0));
for j = 1:4\% gates (1:4)
S(j,i) = calcGateState(S(j,i), Pt(j), k(j)); % fast gates
g(:,i) = calcRect(S(:,i), g(:,i), go, gc, ro, rc, P, vj, Gn);
end % END of channels calculation
gj = sum(gg)./N;
%end % END of gj(vj(t)) calculation
function [S] = calcGateState(S, Pt, k)
% calculate one gate
%S - state of one ch. one gate
if S == 1
pc = Pt*k / (1 + k);
po = 1 - pc;
elseif S == 0
po = Pt*1 / (1 + k);
pc = 1 - po;
tmp = po+pc;
po = po/tmp;
pc = pc/tmp;
end
rr = rand;
```

```
case 1%open
if rr <= po %stay open
%empty
else % go closed
S = 0;
end
case 0% if A is closed
if rr <= po % go to open state
S = 1:
else %stay closed state
%empty
end
end % END of gate state Switching
function \ [g] = calcRect(S, g, go, gc, ro, rc, P, vj, Gn)
% Calculates Rectification
\% g(1:4) - each gates g at i-ch
% vj - vj at t-iteration
g0 = \inf;
w = \inf;
n = 0; % rectification iter. counter
while (w > 1/1000) % calc. rectification until
n = n+1;
gg = 1/(1/g(1)+1/g(2)+1/g(3)+1/g(4)+1/Gn); %recalc. V for
rect.
%v = P.*vj.*gg./g; %voltage on fast gates
v = vj.*gg./g;
for i = 1:2%FAST gates
if S(i) == 1\%open
g(i) = go(i) * exp(v(i)/ro(i)); %includes react.
else %closed
g(i) = gc(i)*exp(v(i)/rc(i)); %includes react.
end
end
for i = 3:4\% SLOW gates
if S(i) == 1\%open
g(i) = go(i); %SLOW gates rect. only OPEN
else %closed
g(i) = gc(i) * exp(v(i)/rc(i)); %includes react.
end
w = abs(g0-gg)/gg; \% diff
g0 = gg;
end
```

An MC16SM of gating

To accelerate the simulation and reduce noise, we developed an MC16SM by transforming an S16SM. Instead of evaluating gating of each individual GI channel, we calculated changes over time of averaged probabilities for each of four gates to be open or closed depending on V_i by using a Markov chain approach. Earlier, we used stationary/steady-state probabilities of Markov chain to model GJ voltage gating (Sakalauskaite et al., 2011; Snipas et al., 2015). However, a steady-state approach is not suitable in this case, because modeling of neuronal networks requires evaluation of dynamic changes in g_r . Thus, we used transitive rather than steady-state probabilities. In doing so, we used a recursive relation, $p^n = p^{n-1} \cdot P$, to calculate the transitive probability vector p^n at a discrete time moment, t_w for each of 16 states, where P denotes the transition probability matrix of a discrete-time Markov chain. Each state s_i can be expressed as a 4-tuple, $s_j = (s_{F,A}; s_{S,A}; s_{S,B}; s_{F,B})$, where each component denotes the state—open (o) or closed (c)—of the respective gate in the GI channel. Thus, the model consists of 16 states, which can be numbered in lexicographical order as follows: $s_1 = (o;o;o;o)$; $s_2 = (o;o;o;c); s_3 = (o;o;c;o); s_4 = (o;o;c;c); s_5 = (o;c;o;o); s_6 = (o;c;o;c);$ $s_7 = (o;c;c;o); s_8 = (o;c;c;c); s_9 = (c;o;o;o); s_{10} = (c;o;o;c); s_{11} =$ $(c;o;c;o); s_{12} = (c;o;c;c); s_{13} = (c;c;o;o); s_{14} = (c;c;o;c); s_{15} = (c;c;c;o);$ and $s_{16} = (c;c;c;c)$.

The transition probabilities among 16 states can be expressed by using the same transition probabilities $p_{o\to c}$ and $p_{c\to o}$ of singular $o\leftrightarrow c$ transitions, as in S16SM. For example, transition probability from s4 = (o,o,c,c) to s_6 = (o,c,o,c), which we denote as $p_{ooc\rightarrow ococ}$, can be estimated as follows: $p_{ooco\rightarrow ococ} = (1 - p_{o\rightarrow c}) \cdot p_{o\rightarrow c} \cdot p_{c\rightarrow o} \cdot (1 - p_{c\rightarrow o})$.

Thus, all basic parameters of the model necessary for building a transition probability matrix P are the same as in the S16SM model, and the same equations are used to estimate K, evaluate I-V rectification, and calculate γ_j . However, because voltage across each gate depends on the state s_j , i.e., $V_F = V_F(s_j)$ and $V_S = V_S(s_j)$, then γ_i must also be evaluated at each state, i.e., $\gamma_i = \gamma_i(s_i)$. Once the transition probability matrix P is formed and the probability vector pⁿ is estimated, then the expected value of junctional conductance g_i is estimated as

$$g_j = \sum_i p_i \cdot \gamma(s_i).$$

We use the following pseudo-code for an implementation of an MC16SM:

```
MC16SM(V_i, p^{tn-1})
begin
1) for each state s_i do
1.1) estimate initial conductance and voltages across each gate;
1.2) Repeat while the values converges
1.2.1) evaluate rectification of conductance of each gate;
1.3) estimate channel conductance at a given state;
1.4) calculate K at estimated voltage values across each gate
1.5) form the i<sup>th</sup> row of matrix P
end for
2) Estimate system probability vector p<sup>n</sup>
3) Estimate expected conductance g_i
return, g_i, \mathbf{p}^n
The MATLAB code of MC16SM:
```

```
function [g_final, q] = MC16SM(yj, par, q)
states = [ 0 0 0 0; 0 0 0 1; 0 0 1 0; 0 0 1 1; ...
0\ 1\ 0\ 0; 0\ 1\ 0\ 1; 0\ 1\ 1\ 0; 0\ 1\ 1\ 1; \dots
1 0 0 0; 1 0 0 1; 1 0 1 0; 1 0 1 1; ...
1 1 0 0; 1 1 0 1; 1 1 1 0; 1 1 1 1];
A = par(:,1);
v0 = par(:,2);
Go = par(:,3);
Gc = par(:,4);
Ro = par(:,5);
Rc = par(:,6);
Pt = par(:,7);
P = par(:,8);
g = zeros(length(states), 4);
v = zeros(length(states), 4);
k = zeros(length(states), 4);
t = zeros(length(states), length(states));
%states conductances
NoRows = size(g,1);
NoCols = size(g,2);
for i = 1:NoRows %g matrix
for j = 1:NoCols
switch(states(i,j))
case 1
g(i,j) = Go(j);
case 0
g(i,j) = Gc(j);
case -1
g(i,j) = Gc(j);
end
end
```

```
g_final = 0;
for ii = 1:4%voltages and rectification
                                                                        NoRows = size(q,1);
                                                                        NoCols = size(q,2);
gg = 1./sum(1./g,2); %sums rows
for i = 1:NoRows %voltages
                                                                        for i = 1:NoRows
for j = 1:NoCols
                                                                        for j = 1:NoCols
v(i,j) = vj*gg(i)/g(i,j);
                                                                        g_{final} = g_{final} + q(i,j) * getG(g,j);
                                                                        end
end
end
                                                                        end
for i = 1:NoRows %conductance according voltage and
                                                                        function gg = getG(g, row)
rectification
                                                                        gg = 1./sum(1./g(row,:)); %sums cols
                                                                        function p = getP(stateFrom, stateTo, k, row, Pt)
for j = 1:NoCols
                                                                        P = 1;
switch(states(i,j))
                                                                        for i = 1:length(stateFrom)
case 1
g(i,j) = Go(j) * exp(v(i,j) / Ro(j));
                                                                        switch(stateFrom(i))
\%go_tmp(ii,1) = g(i,j); \% rekt. braizymui(nebutina)
                                                                        case 1
case 0
                                                                        switch(stateTo(i))
g(i,j) = Gc(j) * exp(v(i,j) / Rc(j));
                                                                        case 1
\%go_tmp(ii,2) = g(i,j); \% rekt. braizymui(nebutina)
                                                                        p = p * (1 - Pt(i) * k(row, i) / (1 + k(row, i)));
end
                                                                        case 0
end
                                                                        p = p * Pt(i) * k(row, i) / (1 + k(row, i));
end
                                                                        case -1
end
                                                                        p = p * 0;
for i = 1:NoRows %k - for next state
                                                                       end
for j = 1:NoCols
                                                                       case 0
k(i,j) = \exp(A(j)*(v(i,j)*P(j)-v0(j)));
                                                                       switch(stateTo(i))
end
                                                                       case 1
end
                                                                        p = p * (Pt(i) / (1 + k(row, i)));
for i = 1:length(states) %Transition matrix
                                                                       case 0
for i = 1:length(states)
                                                                        p = p * ((1 - Pt(i) / (1 + k(row, i))));
t(i,j) = getP(states(i,:),states(j,:),k,i,Pt);
                                                                        end
end
                                                                       end
                                                                       end
end
q = q*t;
```

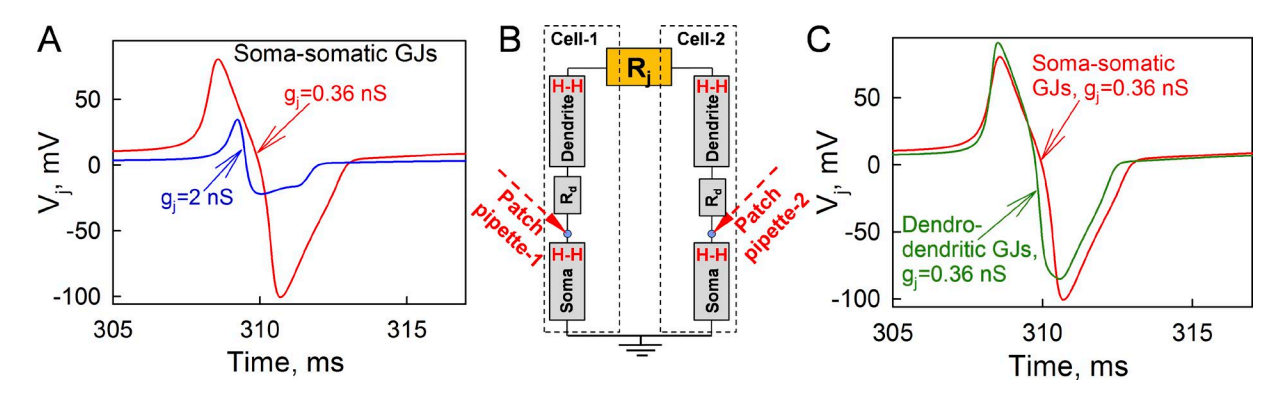


Figure S1. Examples of $V_{j,AP}$ spikes in soma-somatic and dendro-dendritic GJs. This figure is related to Fig. 4. (A) Comparison of $V_{j,AP}$ spikes caused by different junctional conductances between the pair of neurons. The red curve is the same as in the inset of Fig. 4 C (g_j = 0.36 nS). Higher g_j (2 nS) caused shorter delay between APs in neighboring cells, which resulted in shortened and decreased amplitude of $V_{j,AP}$ spike (blue curve). (B) The principal electrical scheme of dendro-dendritic electrical synapse. H-H models for somas and dendritic compartments were the same. R_{d_j} axial resistance of dendritic compartment. (C) Comparison of $V_{j,AP}$ spikes obtained by simulating soma-somatic (red; same as in A) and dendro-dendritic (green) GJs; in both cases, g_j = 0.36 nS and R_d = 500,000 Ohm.

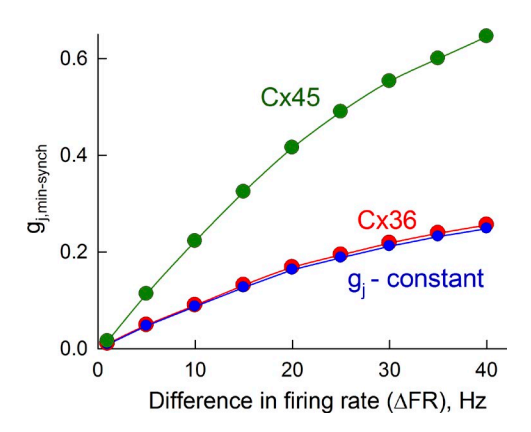


Figure S2. The effect of low and high V_7 -sensitive GJs on $g_{j,min-synch}$ in a cluster of 5 × 5 neurons. This figure is related to Fig. 5. The relationship between $g_{j,min-synch}$ and the difference in spiking rate of neurons interconnected through constant resistance (blue), Cx36 GJs (red), and Cx45 GJs (green). Data show that a difference in $g_{j,min-synch}$ between GJs of constant resistance and those formed of Cx36 are almost identical, whereas $g_{j,min-synch}$ is ~2.2-fold higher when GJs are formed of highly V_7 -sensitive Cx45. In this simulation, the maximum intrinsic firing rate (before synchronization) of neurons was fixed at 100 Hz, which was achieved by applying I_{ext} = 41 pA. The minimum intrinsic firing rate was 60–98 Hz, which was achieved at I_{ext} values of 10–40 pA. Distribution of firing rates among 25 neurons at each value of ΔFR was chosen randomly.

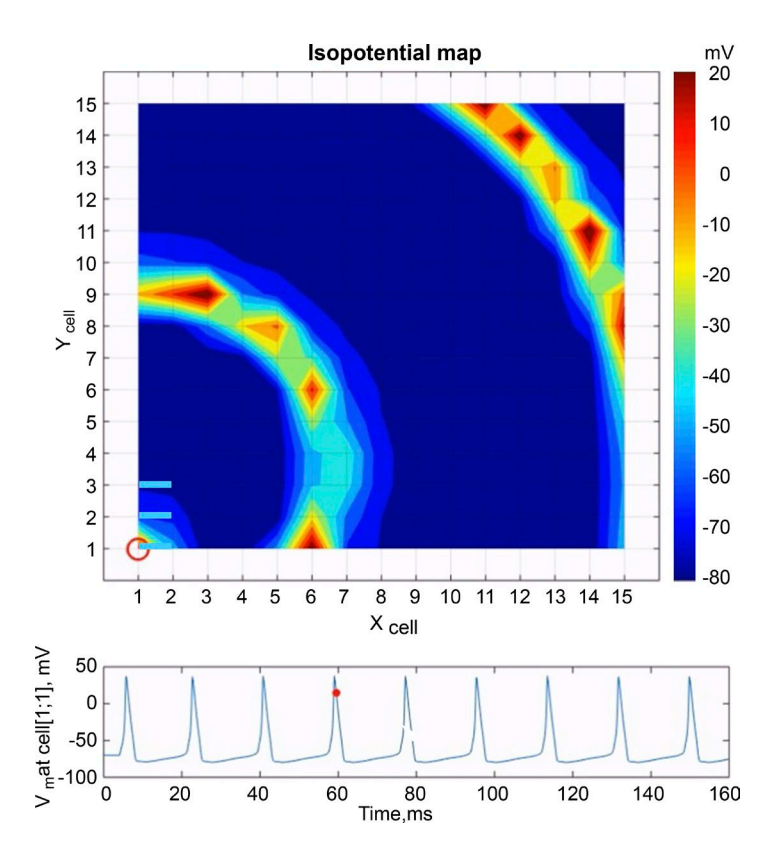


Figure 53. Reverberation of excitation. This figure is related to Fig. 8 and Video 1. Reverberation of excitation in a cluster of 225 neurons (15 rows × 15 columns) interconnected through GJ channels imitating properties of Cx36 and modulatable by an MC16SM. Changes of the membrane potential (V_m) in all cells of the cluster at a particular moment are represented in colors according to the colored bar shown on the right. The reverberation was initiated by a single external stimulus (I_{ext}) applied to cell 1/1 (red circle). Initially, excitation spreads upward to cells 1/2 and 1/3, but not to cells 2/1 and 2/2, because of a local I-V rectification of electrical synapses shown by the light blue segments. Then, excitation returns back to cell 1/1, forming the core of the reverberator. From here, excitation spreads repeatedly over the cluster in the form of spiral waves. Shown at the bottom is a record of the transmembrane potential of cell 1/1. The red dot on the V_m record moves in synchrony with changes of isochrones.

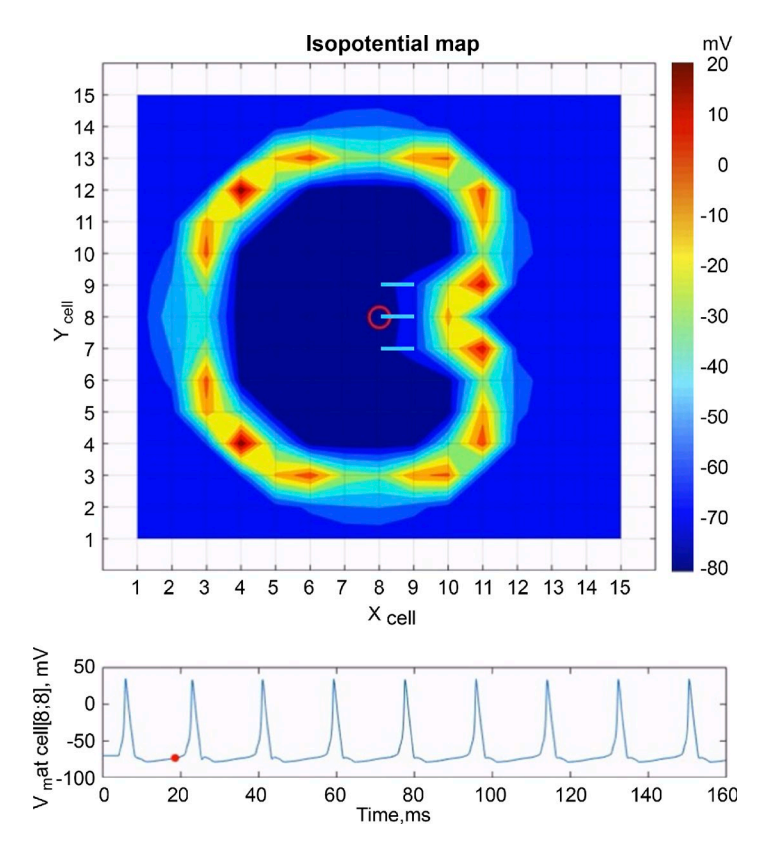


Figure S4. Reverberation of excitation. This figure is related to Fig. 8 and Video 2. The same as in Fig. 8 and Video 1, but the reverberation was initiated by a single stimulus applied to cell 8/8 (red circle). Initially, excitation spreads in all directions, but not to cells 9/9, 9/8, or 9/7, because of a local I-V rectification of electrical synapses indicated by light blue segments. Then, excitation returns back to cell 8/8, forming two reverberators. From here, excitation spreads repeatedly over the cluster in the form of two spiral waves colliding with each other. Shown at the bottom is a record of the transmembrane potential of cell 8/8.

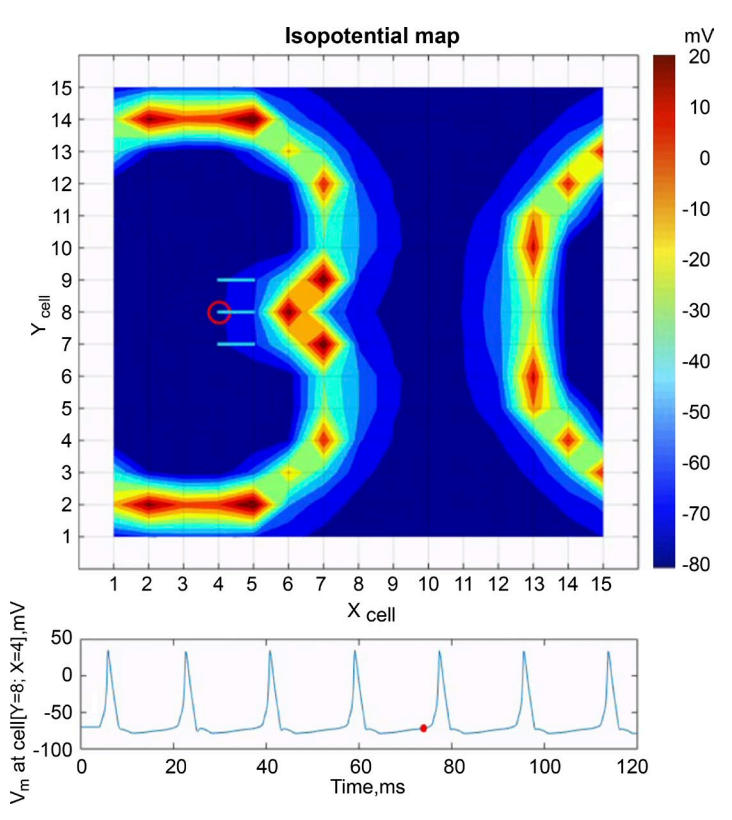


Figure \$5. Reverberation of excitation. This figure is related to Fig. 8 and Video 3. The same as in Fig. 8 and Videos 1 and 2, but the cluster was wrapped on a torus. In doing so, all cells in column 1 are connected with cells in column 15, and all cells in row 1 are connected with cells in row 15. Reverberation was initiated by a single stimulus applied to cell 4/8 (red circle); I-V-rectifying junctions are indicated by light blue segments. Fig. S6 shows the returning wave of excitation from the right to the left. Fig. 8 and Video 3 show that this wave collides with the wave spreading from reverberation core.

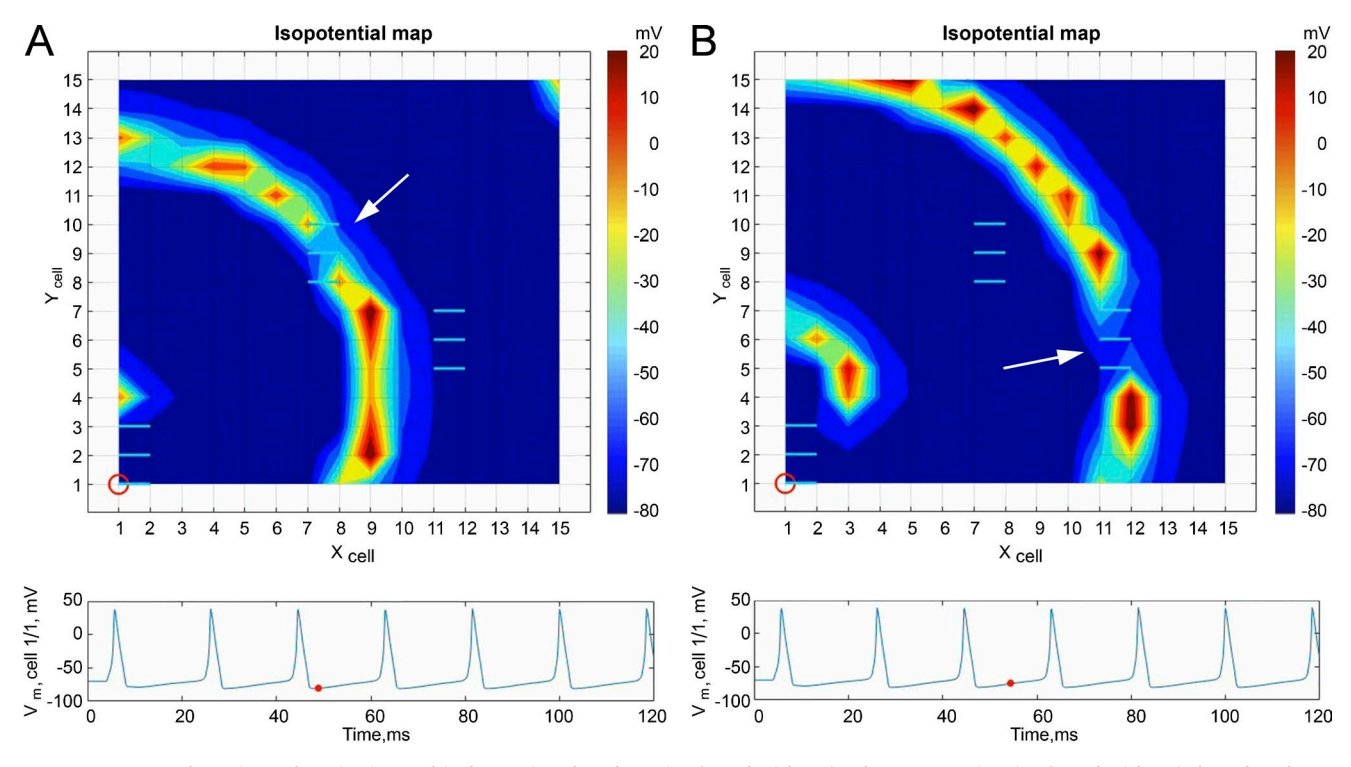
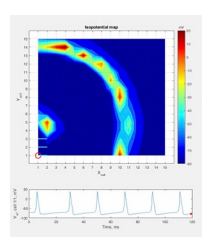
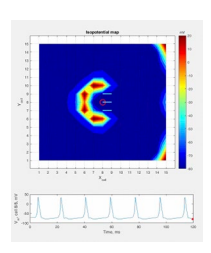


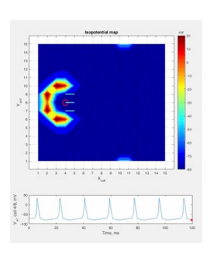
Figure S6. Reverberation of excitation. This figure is related to Fig. 8 and Video 4. The same as in Fig. 8 and Video 1, but the cluster has two additional I-V–rectifying regions (horizontal light blue lines). (A and B) Transformation of spreading spiral wave when passing I-V–rectifying regions in the center (A) and on the right (B) of the cluster (arrows).



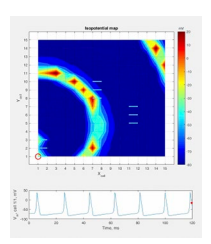
Video 1. Reverberation of excitation in a cluster of 225 neurons (15 rows × 15 columns) interconnected through GJ channels imitating properties of Cx36 and modulatable by an MC16SM. This video is related to Fig. 8 A and Fig. S3. Changes of the membrane potential (V_m) in all cells of the cluster at a particular moment are represented in colors according to the colored bar shown on the right. The reverberation was initiated by a single external stimulus (I_{ext}) applied to cell 1/1 (red circle). Initially, excitation spreads upward to cells 1/2 and 1/3, but not to cells 2/1 and 2/2, because of a local I-V rectification of electrical synapses shown by the light blue segments. Then, excitation returns back to cell 1/1 forming the core of the reverberator. From here, excitation spreads repeatedly over the cluster in the form of spiral waves. Shown at the bottom is a record of the transmembrane potential of cell 1/1. The red dot on the V_m record moves in synchrony with changes of isochrones. Each frame represents 0.5 ms. Frame rate, 30 frames/s.



Video 2. Reverberation of excitation in a cluster of 15×15 neurons. This video is related to Fig. 8 B and Fig. S4. The same as in Video 1, but the reverberation was initiated by a single stimulus applied to cell 8/8 (red circle). Initially, excitation spreads in all directions, but not to cells 9/9, 9/8, and 9/7, because of a local I-V rectification of electrical synapses indicated by light blue segments. Then, excitation returns back to cell 8/8, forming two reverberators. From here, excitation spreads repeatedly over the cluster in the form of two spiral waves colliding with each other. Shown at the bottom is a record of the transmembrane potential of cell 8/8. Each frame represents 0.5 ms. Frame rate, 30 frames/s.



Video 3. Reverberation of excitation in a cluster of 15×15 neurons. This video is related to Fig. 8 and Fig. S5. The same as in Videos 1 and 2, but the cluster was wrapped on a torus. In doing so, all cells in column 1 are connected with cells in column 15, and all cells in row 1 are connected with cells in row 15. Reverberation was initiated by a single stimulus applied to cell 4/8 (red circle); I-V-rectifying junctions are indicated by light blue segments. Shown are the returning wave of excitation spreading from the right to the left and its collision with reverberation core. Each frame represents 0.5 ms. Frame rate, 30 frames/s.



Video 4. Reverberation of excitation in a cluster of 15×15 neurons. This video is related to Fig. 8 A and Fig. S6 (A and B). The same as in Video 1, but the cluster has two additional I-V–rectifying regions (horizontal light blue lines). It shows transformation of a spreading spiral wave when passing I-V–rectifying regions in the center and on the right side of the cluster. Each frame represents 0.5 ms. Frame rate, 30 frames/s.

REFERENCES

- Bukauskas, F.F., A. Bukauskiene, and V.K. Verselis. 2002. Conductance and permeability of the residual state of connexin43 gap junction channels. *J. Gen. Physiol.* 119:171–185. http://dx.doi.org/10.1085/jgp.119.2.171
- Chen-Izu, Y., A.P. Moreno, and R.A. Spangler. 2001. Opposing gates model for voltage gating of gap junction channels. Am. J. Physiol. Cell Physiol. 281:C1604–C1613.
- DeVries, S.H., and E.A. Schwartz. 1992. Hemi-gap-junction channels in solitary horizontal cells of the catfish retina. *J. Physiol.* 445:201–230. http://dx.doi.org/10.1113/jphysiol.1992.sp018920
- Hodgkin, A.L., and A.F. Huxley. 1952. A quantitative description of membrane current and its application to conduction and excitation in nerve. J. Physiol. 117:500–544. http://dx.doi.org/10.1113/ jphysiol.1952.sp004764
- Kronengold, J., E.B. Trexler, F.F. Bukauskas, T.A. Bargiello, and V.K. Verselis. 2003. Pore-lining residues identified by single channel SCAM studies in Cx46 hemichannels. *Cell Commun. Adhes.* 10:193–199. http://dx.doi.org/10.1080/cac.10.4-6.193.199
- Oh, S., J.B. Rubin, M.V. Bennett, V.K. Verselis, and T.A. Bargiello. 1999. Molecular determinants of electrical rectification of single channel conductance in gap junctions formed by connexins 26 and 32. *J. Gen. Physiol.* 114:339–364. http://dx.doi.org/10.1085/jgp.114.3.339
- Palacios-Prado, N., S. Sonntag, V.A. Skeberdis, K. Willecke, and F.F. Bukauskas. 2009. Gating, permselectivity and pH-dependent modulation of channels formed by connexin57, a major connexin of horizontal cells in the mouse retina. *J. Physiol.* 587:3251–3269. http://dx.doi.org/10.1113/jphysiol.2009.171496
- Palacios-Prado, N., S.W. Briggs, V.A. Skeberdis, M. Pranevicius, M.V. Bennett, and F.F. Bukauskas. 2010. pH-dependent modulation of voltage gating in connexin45 homotypic and connexin45/connexin43 heterotypic gap junctions. *Proc. Natl. Acad. Sci. USA*. 107:9897–9902. http://dx.doi.org/10.1073/pnas.1004552107
- Paulauskas, N., M. Pranevicius, H. Pranevicius, and F.F. Bukauskas. 2009. A stochastic four-state model of contingent gating of gap junction channels containing two "fast" gates sensitive to transjunctional voltage. *Biophys. J.* 96:3936–3948. http://dx.doi. org/10.1016/j.bpj.2009.01.059

- Paulauskas, N., H. Pranevicius, J. Mockus, and F.F. Bukauskas. 2012. Stochastic 16-state model of voltage gating of gap-junction channels enclosing fast and slow gates. *Biophys. J.* 102:2471–2480. http://dx.doi.org/10.1016/j.bpj.2012.04.038
- Rackauskas, M., M.M. Kreuzberg, M. Pranevicius, K. Willecke, V.K. Verselis, and F.F. Bukauskas. 2007. Gating properties of heterotypic gap junction channels formed of connexins 40, 43, and 45. *Biophys. J.* 92:1952–1965. http://dx.doi. org/10.1529/biophysj.106.099358
- Sakalauskaite, A., H. Pranevicius, M. Pranevicius, and F. Bukauskas. 2011. Markovian model of the voltage gating of connexin-based gap junction channels. *Electron. Electr. Eng.* 111:103–106.
- Skeberdis, V.A., L. Rimkute, A. Skeberdyte, N. Paulauskas, and F.F. Bukauskas. 2011. pH-dependent modulation of connexin-based gap junctional uncouplers. J. Physiol. 589:3495–3506. http://dx.doi.org/10.1113/jphysiol.2011.209072
- Snipas, M., H. Pranevicius, M. Pranevicius, O. Pranevicius, N. Paulauskas, and F.F. Bukauskas. 2015. Application of stochastic automata networks for creation of continuous time Markov chain models of voltage gating of gap junction channels. *BioMed Res. Int.* 2015:936295. http://dx.doi.org/10.1155/2015/936295
- Tong, J.J., and L. Ebihara. 2006. Structural determinants for the differences in voltage gating of chicken Cx56 and Cx45.6 gap-junctional hemichannels. *Biophys. J.* 91:2142–2154. http://dx.doi.org/10.1529/biophysj.106.082859
- Trexler, E.B., M.V. Bennett, T.A. Bargiello, and V.K. Verselis. 1996. Voltage gating and permeation in a gap junction hemichannel. *Proc. Natl. Acad. Sci. USA*. 93:5836–5841. http://dx.doi.org/10.1073/pnas.93.12.5836
- Valiunas, V., R. Mui, E. McLachlan, G. Valdimarsson, P.R. Brink, and T.W. White. 2004. Biophysical characterization of zebrafish connexin35 hemichannels. Am. J. Physiol. Cell Physiol. 287:C1596–C1604. http://dx.doi.org/10.1152/ajpcell.00225.2004
- Vogel, R., and R. Weingart. 1998. Mathematical model of vertebrate gap junctions derived from electrical measurements on homotypic and heterotypic channels. J. Physiol. 510:177–189. http:// dx.doi.org/10.1111/j.1469-7793.1998.177bz.x